This article has been accepted for publication in a future issue of this journal, but has not been fully edited. Content may change prior to final publication. Citation information: DOI10.1109/TWC.2022.3140268, IEEE Transactions on Wireless Communications

Self-Sustainable Reconfigurable Intelligent Surface Aided Simultaneous Terahertz Information and Power Transfer (STIPT)

Yijin Pan, Kezhi Wang, Cunhua Pan, Huiling Zhu and Jiangzhou Wang, *Fellow, IEEE*

***Abstract*—This paper proposes a new simultaneous terahertz (THz) information and power transfer (STIPT) system, which utilizes a reconfigurable intelligent surface (RIS) for both the data and power transmission. We aim to maximize the information users' (IUs') sum data rate while guaranteeing the power harvesting requirements of energy users (EUs) and RIS. To solve the formulated non-convex problem, the block coordinate descent (BCD) based algorithm is adopted to alternately optimize the transmit precoding of IUs, RIS's reflecting coefficients, and the position of RIS. Additionally, the penalty constrained convex approximation (PCCA) algorithm is proposed to optimize the deployment of the RIS, where the introduced penalties ensure that the solution is always feasible. The simulation results show that the proposed solution outperforms the benchmark schemes, and the proposed BCD algorithm can greatly improve the performance of the STIPT system.**

***Index Terms*—Simultaneous terahertz information and power transfer (STIPT), intelligent reflecting surface (IRS), reconfigurable intelligent surface (RIS), terahertz (THz) communications.**

I. Introduction

Currently, wireless power harvesting (WPH) technology is viewed as a promising approach for self-sustaining devices [1]. Specifically, WPH enables devices to reap power directly from external radio frequency sources [2]. Due to these benefits, numerous Internet of things (IoT) gadgets and sensors are manufactured with the WPH power supply function [3]. Nevertheless, conventional low-frequency radio may no longer be suitable for WPH [4] in small-scale IoT devices, e.g., the nanoscale IoT devices. The low-frequency radio wave normally requires a large antenna aperture due to its relatively large wavelength [5], and the large aperture of the required rectennas easily exceeds the size restriction of IoT devices [6]. One possible solution is to increase the radio frequency. Thus, by using shorter wavelengths, rectennas can be greatly reduced in size [4].

Meanwhile, current mobile network is expected to provide extremely high data rate for realizing a variety of multimedia services [7]. Thanks to the enormous spectrum resources in the terahertz (THz) band, THz transmission can achieve data rates from hundreds of Gbps to several Tbps. As a result, THz communication is envisioned as a potential option for meeting the ultra-high rate requirements of enhanced mobile broadband (eMBB) services such as virtual reality [8]. Furthermore, as the THz band spans from 100 GHz to 10 THz, the wavelength of THz can considerably reduce the necessary antenna aperture [9]. Consequently, utilizing the THz radios for wireless power harvesting becomes an attractive approach [10], [11]. As a result, combining the benefits of the THz transmission in providing high-speed data rates with WPH for IoT devices will be a promising research direction, leading to the new system: Simultaneous Terahertz Information and Power Transfer (STIPT).

However, due to the relatively short wavelengths of THz signals, obstructions in their propagation paths tend to absorb rather than reflect the THz signals. Thus, THz links are readily blocked by obstacles in transmission paths, resulting in a reduction of THz transmission distance. To address this issue, reconfigurable intelligent surface (RIS), also known as an intelligent reflective surface (IRS), has been leveraged to help compensate for the blocked communication links [12]. More importantly, with the carefully tuned reflecting phase shifts, the RIS can help constructively accumulate significant power at the target receiver. Thus, by carefully adjusting the reflecting coefficients of RIS, the propagation channel condition can be greatly improved for target receivers so that system performance can be enhanced [13].

A. Related Works

Extensive efforts have been devoted to numerous applications of the RIS-assisted transmissions [14]. A comprehensive survey about these applications of the RIS has been given in [15], and the potential benefits from RIS have been explained in various aspects in [16]. In [17], the RIS has been exploited to enhance the cell-edge performance in multicell MIMO communication systems. Also, the RIS was utilized to enhance the latency performance of the mobile edge computing (MEC) system in [18]. Furthermore, the RIS was leveraged to enhance the physical layer security by improving the secrecy rate [19]–[23] and reducing the transmit power [24]. The RIS-enhanced orthogonal frequency division multiplexing (OFDM) system and its corresponding transmission protocol were investigated in [25].

The RIS is envisioned to be a necessity for future THz communications to bypass blockages [26]. To date, many efforts have been devoted to the use of RIS to enhance the THz transmission performance [27], [28]. For instance, the

Corresponding authors: Cunhua Pan and Kezhi Wang. Y. Pan and C. Pan are with the National Mobile Communications Research Laboratory, Southeast University, Nanjing 211111, China. K. Wang is with the Department of Computer and Information Sciences, Northumbria University, UK. J. Wang and H. Zhu are with the School of Engineering and Digital Arts, University of Kent, UK.

This article has been accepted for publication in a future issue of this journal, but has not been fully edited. Content may change prior to final publication. Citation information: DOI10.1109/TWC.2022.3140268, IEEE Transactions on Wireless Communications

RIS was utilized in [29] to enhance the THz coverage. The channel estimation by beam training and hybrid beamforming design were investigated in [30] for the RIS-assisted THz channel. The weighted sum rate was maximized in [31] by jointly optimizing the hybrid beamforming and reflecting matrix of the RIS. The THz channel fading characteristics was exploited in [32] to optimize the trajectory for a RIS-assisted UAV system. The sum rate was maximized in [33] with the consideration of the frequency-selective THz channel.

The application of RIS has also been investigated in the simultaneous wireless information and power transfer (SWIPT) system [34]. For example, a RIS-aided MIMO broadcasting SWIPT system was investigated in [35], where the transmit precoding matrices and passive phase shift matrix of the RIS were jointly optimized to maximize the weighted sum rate of information users while guaranteeing the users' energy harvesting requirement. The active and passive beamforming were investigated in [36] for the constant-envelope wireless power transfer (WPT) system, and the results in [36] revealed that the average received power increases quadratically with the number of RIS elements. The contributions in [37] investigated the RIS-aided secure transmission system, where the energy efficiency was enhanced by optimizing the reflecting coefficients of RIS. In [38], RIS was leveraged to enhance the performance of non-orthogonal multiple access (NOMA) WPT efficiency. The energy harvesting efficiency of the RIS-assisted MIMO broadcasting SWIPT system was investigated in [39], where the required transmit power was minimized while satisfying the QoS constraints. A RIS-assisted WPT OFDM system was investigated in [40], where the energy consumption was minimized by leveraging tunable RIS.

B. Motivations and Contributions

Compared to traditional micro/millimetre wave transmission, the THz signal suffers from non-negligible atmospheric attenuation caused by molecule absorption. As a result, multiple path loss peaks arise in the THz band [41]. The entire THz band is then divided into several sub-bands with different central frequencies. In this case, the phases of incident waveforms are different across the sub-bands [33]. This makes the RIS phase shift matrix difficult to design since the phase shifts of the RIS reflecting elements must be properly tuned for the balance of many sub-bands. Furthermore, the precoding for different users needs to be revisited carefully on the multiple THz sub-bands. Nonetheless, in most of the above-mentioned RIS-SWIPT approaches [34]–[40], the THz band's specific channel characteristics were not taken into account.

In addition, the path losses on different sub-bands are sensitive to the link distances [42], which is highly dependent on the location of RIS. Specifically, in the STIPT system with weak LOS paths, the RIS-assisted channels contribute significantly to the received signal. However, in the aforementioned RIS-THz systems [29]–[32], the deployment location of RIS was not addressed. In a typical STIPT application scenario, the energy users are usually IoT devices or sensors, while the information users are deployed for the monitoring tasks such as transmitting high-definition video/figures that entail ultra-high data rates. In this case, the locations of these user equipments can be predicted according to the indoor layout or the historical statistics of UEs' locations [43]. Consequently, in this scenario, where users' positions are relatively fixed, the information of UEs' locations can be exploited at the AP. The optimization of RIS deployment in this STIPT system can effectively compensate for the link-distance dependent fading in the THz band, which was not addressed in the current RIS-SWIPT approaches [35]. However, optimizing the location of RIS with power constraints is challenging due to multiple periodic cosine components in the channel expression, and currently, no efficient solutions have been reported in the literature, to the best of our knowledge.

Additionally, to improve the reflectivity performance of the high-frequency THz radios, the number of RIS elements in the STIPT can be greatly increased. As a result, the energy consumption of RIS would considerably increase as well [44], which cannot be ignored in the STIPT system. However, in the works mentioned above [25], [33], the RIS is assumed to be powered by fixed charging lines, and hence the RIS's power consumption is often neglected. In many application scenarios, additional costs for wired power supply may be necessary, and it can restrict the deployment flexibility of RIS. Another direction is to power the RIS by using wireless power transfer technology. However, it is currently unclear how to power the self-sustaining RIS while preserving the EU's circuit power consumption and IU's information transmission.

Taking into account the aforementioned challenges, we aim to develop an effective STIPT communication system in this work by addressing the impact of the THz frequency-selective channel on the RIS reflection phase design and RIS deployment. To be more explicit, we investigate the STIPT system's downlink transmission, where the RIS-assisted THz links serve both information users (IUs) and energy users (EUs). The wireless-powered RIS harvests energy from received THz radios to power its own circuits. The IU precoding, the RIS reflecting coefficients, and the RIS coordinate are jointly optimized in order to maximize the achievable rates of the IUs while meeting the EU and RIS power harvesting requirements. Overall, our contributions can be summarized as follows:

- We propose a RIS-aided STIPT system to simultaneously transmit information and power for IUs and EUs, respectively. Wireless powered RIS helps the information transmission and power transfer in a self-sustaining manner. The power harvested by RIS can be adjusted by tuning the amplitude of reflecting coefficients. The RIS-assisted THz channel is modelled as a function of the RIS reflecting coefficients and the coordinate of RIS.
- The optimization problem is formulated to maximize the IUs' sum rates while guaranteeing the power harvesting requirements of the EUs. The original non-convex problem is first reformulated by utilizing the equivalence between the weighted minimum mean-square error (WMMSE) and the signal to interference-plus-noise ratio (SINR). The block coordinate descent (BCD) based algorithm is proposed to alternately optimize the precoding for IUs, RIS's reflecting coefficients and RIS's coordinate.

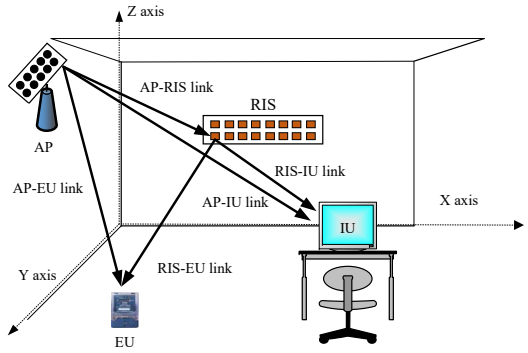

Fig. 1. The RIS-assisted SWIFT system.

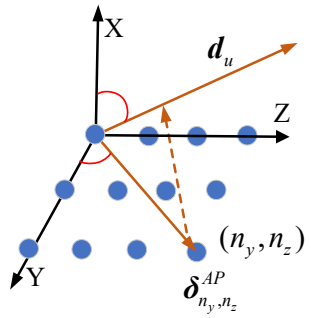

Fig. 2. Phase difference between AP's antenna elements.

- The precoding for IUs and RIS's reflecting coefficients are obtained by utilizing the successive convex approximation method. To deal with the intractable optimization problem of the RIS's coordinate, we propose the penalty constrained convex approximation (PCCA) algorithm to guarantee the solution's feasibility and the monotonicity of objective value.

The remainder of this paper is organized as follows: Section II describes the system model of the proposed RIS-aided STIPT system and formulates the optimization problem. Section III develops the detailed algorithm to solve the formulated sum-rate maximization problem. In Section IV, the simulation results are presented to show the performance gain and the impact of system parameters, whereas Section V concludes the paper.

Notation: For vector $\boldsymbol{x}$, $|\boldsymbol{x}|$ and $(\boldsymbol{x})^T$ respectively denote its Euclidean norm and its transpose. c represents the light speed. For matrix $\boldsymbol{A}$, $\boldsymbol{A}^*$ and $\boldsymbol{A}^\star$ represent the conjugate operator and converged solution, respectively. $\mathbb{C}^{M\times 1}$ denotes the set of $M \times 1$ complex vectors. $\text{diag}(\boldsymbol{X})$ represents the vector that is obtained from the diagonal entries of matrix $\boldsymbol{X}$. $\boldsymbol{a} \odot \boldsymbol{b}$ represents the Hadamard (point-wise) product of $\boldsymbol{a}$ and $\boldsymbol{b}$.

II. System Model and Problem Formulation

Consider the downlink of a STIPT system that serves the IoT sensors and video transmission devices at the same time, as shown in Fig. 1. The network access point (AP) operates in the THz band. EUs are IoT sensors and they need to harvest power from the THz radio, meanwhile, IUs require high-speed data transmission for high-definition video/figures. As the THz channel is frequency-selective, the total THz band is divided into K sub-bands (SBs). Let f_k denote the central frequency of SB k, and its wavelength is given by $\lambda_k = \frac{c}{f_k}$.

The AP is equipped with N_t transmit antennas to serve I IUs and M EUs, and all of which are equipped with N_r receive antennas. Let $\mathcal{I}$ and $\mathcal{M}$ respectively represent the set of IUs and EUs. Then, the set of all users is given by $\mathcal{U} = \mathcal{I} \cup \mathcal{M}$, and the total number of all users (including EUs and IUs) is denoted by $U = |\mathcal{U}|$. In the following, user u can be referred to either an EU or an IU.

Due to the extremely short wavelength of the THz radio, the surfaces of walls and ceilings appear "rough" to THz signals. In other words, they absorb and scatter THz signals rather than reflecting them in the desired direction [8], [45]. Also, as concluded in [46], the average additional attenuation per reflection in THz band is expected to be 12–13 dB. As a result, second-bounce or more reflections and scattering components are severely attenuated and thus play insignificant roles in the received signal power. Consequently, similar to [31], [47], [48], we neglect the effects of random reflections, scattering, and only consider the LOS components of the AP-user links, the AP-RIS link and the RIS-user links.

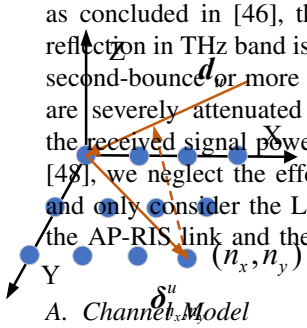

A. Channel Model

We first consider the LOS paths for the AP-user u link. Denote the coordinate of the $(0,0)$th AP antenna and the $(0,0)$th antenna of user u as $\boldsymbol{s}_{AP}$ and $\boldsymbol{s}_u \in \mathbb{R}^{3\times 1}$, respectively, so that the transmit vector from AP to user u is $\boldsymbol{d}_u = \boldsymbol{s}_u - \boldsymbol{s}_{AP}$. In the far-field region of the AP, there is a phase difference of the incident signal sent across the AP antenna elements. As shown in Fig. 2.(a), the phase difference of the (n_y, n_z)th AP antenna element compared to the $(0,0)$th antenna element for user u is given by

$$\theta_{k,u}(n_y, n_z) = \frac{2\pi f_k}{c} \frac{\boldsymbol{d}_u^T \boldsymbol{\delta}^{AP}_{n_y,n_z}}{|\boldsymbol{d}_u|}, \tag{1}$$

where $\boldsymbol{\delta}^{AP}_{n_y,n_z}$ is the directional vector from the (n_y, n_z)th AP antenna to the $(0,0)$th AP antenna as shown in Fig. 2. Then, the transmit array vector from the AP to user u on SB k is denoted by

$$\boldsymbol{v}_{k,u} = [1, \cdots, \exp(-j\theta_{k,u}(n_t)), \cdots, \exp(-j\theta_{k,u}(N_t-1))]^T, \tag{2}$$

where $n_t = n_y + n_z N_Y^{AP}, n_y = 0, \cdots, N_Y^{AP} - 1, n_z = 0, \cdots, N_Z^{AP} - 1$ and $N_Z^{AP} N_Y^{AP} = N_t$.

Similarly, when user u is in the XOY plane, the phase difference of the receive signal between the $(0,0)$th antenna element and the (n_x, n_y)th antenna of user u is calculated as

$$\varrho_{k,u}(n_x, n_y) = \frac{2\pi f_k}{c} \frac{\boldsymbol{d}_u^T \boldsymbol{\delta}^{u}_{n_x,n_y}}{|\boldsymbol{d}_u|}, \tag{3}$$

where $\boldsymbol{\delta}^{u}_{n_x,n_y}$ is the directional vector from the (n_x, n_y)th antenna element to the $(0,0)$th antenna element. Then, the receive array response at user u for the AP on SB k is

$$\boldsymbol{r}^{dir}_{k,u} = [1, \cdots, \exp(-j2\pi f_k \varrho_{k,u}(n_r)), \cdots, \exp(-j2\pi f_k \varrho_{k,u}(N_r - 1))]^T, \tag{4}$$

This article has been accepted for publication in a future issue of this journal, but has not been fully edited. Content may change prior to final publication. Citation information: DOI10.1109/TWC.2022.3140268, IEEE Transactions on Wireless Communications

where $n_r = n_x + n_y N_X^u$,$n_x = 0, \cdots, N_X^u - 1$,$n_y = 0, \cdots, N_Y^u - 1$ and $N_X^u N_Y^u = N_r$.

According to the ray tracing techniques [49], the path gain from the AP to user u on SB k is evaluated as

$$h_{k,u} = \left(\frac{G_r G_t \lambda_k}{4\pi |\boldsymbol{d}_u|}\right) \exp\left(-j2\pi \frac{|\boldsymbol{d}_u|}{\lambda_k}\right) \exp\left(-\frac{1}{2} K(f_k) |\boldsymbol{d}_u|\right), \tag{5}$$

where G_r and G_t respectively represent the antenna gain of transmit array and the antenna gain of receiving array, and $K(f_k)$ is the overall absorption coefficient of the transmission medium on SB k. Then, the LOS channel components of the AP-user u link are denoted as

$$\boldsymbol{H}_{k,u}^{LOS} = h_{k,u} \boldsymbol{r}_{k,u}^{dir} \boldsymbol{v}_{k,u}^H, u \in \mathcal{I} \cup \mathcal{M}. \tag{6}$$

B. RIS Assisted Links

The number of reflecting elements of the RIS is denoted as N. As the RIS-assisted links are already single-bounce reflected rays, we only consider the direct paths of AP-RIS and RIS-users links. In this case, the transmit array vectors for the RIS assisted links depends on the RIS's coordinate $\boldsymbol{l} = [x, y, z]^T$, which is evaluated at the $(0,0)$th RIS element.

As the transmit vector from AP to the RIS is $\boldsymbol{d}_0(\boldsymbol{l}) = \boldsymbol{l} - \boldsymbol{s}_{AP}$, the transmit distance between the AP and the RIS is evaluated as $d_0(\boldsymbol{l}) = |\boldsymbol{d}_0(\boldsymbol{l})|$. Similar to (1), the phase difference send from AP to the RIS is calculated as

$$\theta_k(n_y, n_z) = \frac{2\pi}{\lambda_k} \frac{\boldsymbol{d}_0(\boldsymbol{l})^T \boldsymbol{\delta}_{n_y,n_z}^{AP}}{d_0(\boldsymbol{l})}. \tag{7}$$

where $\theta_k(n_y, n_z)$ denotes the phase different between the the $(0,0)$th AP antenna element and the (n_y, n_z)th element on SB k. Then, the transmit array vector from the AP to the RIS on SB k is then denoted by

$$\boldsymbol{v}_k = [1, \cdots, \exp(-j2\pi f_k \theta_k(n_t)), \cdots, \exp(-j2\pi f_k \theta_k(N_t - 1)]^T, \tag{8}$$

where $n_t = n_y + n_z N_Y^{AP}$,$n_y = 0, \cdots, N_Y^{AP} - 1$,$n_z = 0, \cdots, N_Z^{AP} - 1$ and $N_Z^{AP} N_Y^{AP} = N_t$.

Furthermore, because the transmit distance between the RIS elements varies, we define a receiving array vector $\boldsymbol{e}_k$ for the RIS on SB k. Suppose that the RIS is placed on the XOZ plane. Let $\boldsymbol{\delta}_{n_x,n_z}^{RIS}$ denote the directional vector from the (n_x, n_z)th RIS element to the $(0,0)$th RIS element. Then, phase difference of the received signals between the RIS elements is

$$\vartheta_k(n_x, n_z) = \frac{2\pi}{\lambda_k} \frac{\boldsymbol{d}_0(\boldsymbol{l})^T \boldsymbol{\delta}_{n_x,n_z}^{RIS}}{d_0(\boldsymbol{l})}, \tag{9}$$

where $\boldsymbol{\delta}_{n_x,n_z}^{RIS}$ is the directional vector from the (n_x, n_z)th RIS element to the $(0,0)$th RIS element. In addition, $n_x = 0, \cdots, N_X^{RIS} - 1$,$n_z = 0, \cdots, N_Z^{RIS} - 1$ and $N_Z^{RIS} N_Y^{RIS} = N$. Then, the receive array vector at the RIS of the AP-RIS link is given by

$$\boldsymbol{e}_k = [1, \cdots, \exp(-j\vartheta_k(n)), \cdots, \exp(-j\vartheta_k(N-1))]^T, \tag{10}$$

where $n = n_x + n_z N_X^{RIS}$, $n_x = 0, \cdots, N_X^{RIS} - 1$, $n_z = 0, \cdots, N_Z^{RIS} - 1$ and $N_Z^{RIS} N_X^{RIS} = N$.

As the path-loss gain from the AP to the RIS on SB k is evaluated as

$$H_k = \left(\frac{G_t \lambda_k}{4\pi d_0(\boldsymbol{l})}\right) \exp\left(-j2\pi \frac{d_0(\boldsymbol{l})}{\lambda_k}\right) \exp\left(-\frac{1}{2} K(f_k) d_0(\boldsymbol{l})\right), \tag{11}$$

then the LOS channel of the AP-RIS link on SB k is denoted by

$$\boldsymbol{H}_k = H_k \boldsymbol{e}_k \boldsymbol{v}_k^H. \tag{12}$$

Then, we consider the RIS-user u link. The transmit distance between the RIS and user u is evaluated as $d_{0,u}(\boldsymbol{l}) = |\boldsymbol{d}_{0,u}(\boldsymbol{l})|$, where $\boldsymbol{d}_{0,u}(\boldsymbol{l}) = \boldsymbol{s}_u - \boldsymbol{l}$. Similarly, the transmit phase difference between the RIS elements is

$$\vartheta_{k,u}(n_x, n_z) = \frac{2\pi}{\lambda_k} \frac{\boldsymbol{d}_{0,u}(\boldsymbol{l})^T \boldsymbol{\delta}_{n_x,n_z}^{RIS}}{d_{0,u}(\boldsymbol{l})}, \tag{13}$$

and the transmit array vector from the RIS to user u on SB k is expressed as

$$\boldsymbol{e}_{k,u} = [1, \cdots, \exp(-j\vartheta_{k,u}(n)), \cdots, \exp(-j\vartheta_{k,u}(N-1))]^T. \tag{14}$$

where $n = n_x + n_z N_X^{RIS}$, $n_x = 0, \cdots, N_X^{RIS} - 1$, $n_z = 0, \cdots, N_Z^{RIS} - 1$ and $N_Z^{RIS} N_X^{RIS} = N$.

As the power consumption of the RIS cannot be ignored, we assume that the WPH module is equipped in the RIS so that the RIS can also harvest energy from the radios sent by the AP. As a result, the reflecting coefficient is denoted by $\Phi_n = \beta_n \exp(j\phi_n)$, where β_n and ϕ_n respectively represent the amplitude and the phase shift of the n-th reflecting element. Then, the phase shift matrix of the RIS is denoted by

$$\boldsymbol{\Phi} = \text{diag}\{\beta_n \exp(j\phi_n), n = 1, \cdots, N\}. \tag{15}$$

We then have the following constraints for the reflecting coefficients as

$$C1 : |\beta_n \exp(j\phi_n)| \leq 1, n = 1, \cdots, N. \tag{16}$$

In addition, the receive phase difference at user u's different antenna elements of the RIS-user u link is

$$\zeta_{k,u}(n_x, n_y) = \frac{2\pi}{\lambda_k} \frac{\boldsymbol{d}_{0,u}(\boldsymbol{l})^T \boldsymbol{\delta}_{n_x,n_y}^{u}}{d_{0,u}(\boldsymbol{l})}. \tag{17}$$

Then, the receive array vector at user u on SB k of the RIS-user u link is expressed as

$$\boldsymbol{r}_{k,u} = [1, \cdots, \exp(-j\zeta_{k,u}(n_r)), \cdots, \exp(-j\zeta_{k,u}(N_r - 1))]^T, \tag{18}$$

where $n_r = n_x + n_y N_X^u$,$n_x = 0, \cdots, N_X^u - 1$,$n_y = 0, \cdots, N_Y^u - 1$ and $N_X^u N_Y^u = N_r$.

The cascaded channel gain of the AP-RIS-user u link on SB k can be expressed as [50]

$$g_{k,u} = \left(\frac{G_t G_r \lambda_k}{8\sqrt{\pi^3} d_{0,u}(\boldsymbol{l}) d_0(\boldsymbol{l})}\right) \exp\left(-j2\pi \frac{d_{0,u}(\boldsymbol{l}) + d_0(\boldsymbol{l})}{\lambda_k}\right) \exp\left(-\frac{1}{2} K(f_k)(d_{0,u}(\boldsymbol{l}) + d_0(\boldsymbol{l}))\right), \tag{19}$$

where $|\boldsymbol{d}_{0,u}|$ and $|\boldsymbol{d}_0|$ represent the distance from the RIS to the user u and the AP, respectively. Overall, the AP-RIS-user u link on SB k is given by

$$\boldsymbol{G}_{k,u} = g_{k,u} \boldsymbol{r}_{k,u} \boldsymbol{e}_{k,u}^H \boldsymbol{\Phi} \boldsymbol{e}_k \boldsymbol{v}_k^H, u \in \mathcal{I} \cup \mathcal{M}. \tag{20}$$

This article has been accepted for publication in a future issue of this journal, but has not been fully edited. Content may change prior to final publication. Citation information: DOI10.1109/TWC.2022.3140268, IEEE Transactions on Wireless Communications

C. Information Transfer

The signal vector transmitted from the AP to IU i on SB k is $\boldsymbol{s}_{k,i} \in \mathbb{C}^{d\times 1}$. Suppose that the data symbol $\boldsymbol{s}_{k,i}$ satisfies $\mathbb{E}[\boldsymbol{s}_{k,i}\boldsymbol{s}_{k,i}^H] = \boldsymbol{I}_d$ and $\mathbb{E}[\boldsymbol{s}_{k,i}\boldsymbol{s}_{k,j}^H] = \boldsymbol{0}$ for $i \neq j$. Let $\boldsymbol{F}_{k,i} \in \mathbb{C}^{N_t\times d}$ denote the precoding matrix used by the AP for IU i on SB k. Then, the transmitted signal $\boldsymbol{x}_k \in \mathbb{C}^{N_t\times 1}$ from the AP on SB k is

$$\boldsymbol{x}_k = \sum_{i=1}^{I} \boldsymbol{F}_{k,i}\boldsymbol{s}_{k,i}. \tag{21}$$

With the aid of the RIS, the received signal at IU i on SB k is

$$\boldsymbol{y}_{k,i} = (\boldsymbol{H}_{k,i} + \boldsymbol{G}_{k,i})\boldsymbol{x}_k + \boldsymbol{n}_{k,i} = \boldsymbol{Z}_{k,i}\boldsymbol{x}_k + \boldsymbol{n}_{k,i}, \tag{22}$$

where $\boldsymbol{Z}_{k,i} = \boldsymbol{H}_{k,i} + \boldsymbol{G}_{k,i}$, and $\boldsymbol{n}_{k,i}$ is the additive Gaussian noise.

Then, the achievable data rate of IU i on SB k is given by

$$R_{k,i} = \log\left|\boldsymbol{I}_{N_r} + \boldsymbol{F}_{k,i}^H\boldsymbol{Z}_{k,i}^H\boldsymbol{Z}_{k,i}\boldsymbol{F}_{k,i}\boldsymbol{J}_{k,i}^{-1}\right|, \tag{23}$$

where $|\boldsymbol{X}|$ stands for the determinant of matrix $\boldsymbol{X}$, $\boldsymbol{J}_{k,i} = \sum_{u\neq i}^{I}\boldsymbol{Z}_{k,i}\boldsymbol{F}_{k,u}\boldsymbol{F}_{k,u}^H\boldsymbol{Z}_{k,i}^H + \sigma_{k,i}^2\boldsymbol{I}_{N_r}$, and $\sigma_{k,i}^2$ is the noise power.

Furthermore, as the transmit power is limited, we have the following constraints for the precoding matrices:

$$C2: \sum_{k=1}^{K}\sum_{i=1}^{I}\|\boldsymbol{F}_{k,i}\|_F^2 \leq P_T^{max}. \tag{24}$$

D. Energy Harvesting

As the RIS also harvests energy from the AP, so that the reflecting coefficients can be adjusted to satisfy the energy harvesting requirement. That is to say, a part of the AP's energy is reflected by the RIS, and the remaining part is fed into the RIS's WPH unit for harvesting. For the power harvested at the RIS, we only account for the power received from the transmitted wireless signals and ignore the additive white Gaussian noise $\boldsymbol{n}_{k,i}^{RIS}$ as it is insignificant compared with the former. The received signal at the RIS for IU i on SB k is given by $\boldsymbol{y}_{RIS}^{in} = \boldsymbol{H}_k\boldsymbol{F}_{k,i} + \boldsymbol{n}_{k,i}^{RIS}$. Consequently, the power received by the RIS on SB k is

$$q_k^{in} = \sum_{i=1}^{I}||\boldsymbol{H}_k\boldsymbol{F}_{k,i}||_F^2 = \sum_{i=1}^{I}\mathrm{tr}\left(\boldsymbol{F}_{k,i}^H\boldsymbol{H}_k^H\boldsymbol{H}_k\boldsymbol{F}_{k,i}\right). \tag{25}$$

In addition, the signal reflected from the RIS to IU i on SB k is $\boldsymbol{y}_{RIS}^{out} = \boldsymbol{\Phi}\boldsymbol{H}_k\boldsymbol{F}_{k,i} + \boldsymbol{n}_{k,i}^{RIS}$. Consequently, the reflected power by the RIS on SB k is

$$q_k^{out} = \sum_{i=1}^{I}||\boldsymbol{\Phi}\boldsymbol{H}_k\boldsymbol{F}_{k,i}||_F^2 = \sum_{i=1}^{I}\mathrm{tr}\left(\boldsymbol{F}_{k,i}^H\boldsymbol{H}_k^H\boldsymbol{\Phi}^H\boldsymbol{\Phi}\boldsymbol{H}_k\boldsymbol{F}_{k,i}\right). \tag{26}$$

Then, the harvested power by the RIS is calculated by

$$P_{RIS} = \sum_{k=1}^{K}\eta_k(q_k^{in} - q_k^{out}). \tag{27}$$

where η_k denotes the power harvesting efficiency on SB k, since the RF-DC conversion efficiency depends on the carrier's frequency [51]. Let P^I denote the required power for RIS, then we have

$$C3: \sum_{k=1}^{K}\sum_{i=1}^{I}\eta_k\mathrm{tr}\left(\boldsymbol{F}_{k,i}^H\boldsymbol{H}_k^H(\boldsymbol{I} - \boldsymbol{\Phi}^H\boldsymbol{\Phi})\boldsymbol{H}_k\boldsymbol{F}_{k,i}\right) \geq P^I. \tag{28}$$

Similarly, the power harvested by EU m should satisfy the following constraint:

$$C4: \sum_{k=1}^{K}\sum_{i=1}^{I}\eta_k\mathrm{tr}\left(\boldsymbol{Z}_{k,m}\boldsymbol{F}_{k,i}\boldsymbol{F}_{k,i}^H\boldsymbol{Z}_{k,m}^H\right) \geq P_m^U, m \in \mathcal{M}, \tag{29}$$

where P_m^U is the required power of EU m, and $\boldsymbol{Z}_{k,m}$ is the composite channel gain between the AP and the EU m on SB k.

E. Problem Formulation

For ease of presentation, we define $\boldsymbol{\beta} = [\beta_1, \cdots, \beta_N]$ as the amplitude vector of the reflecting coefficients, and define $\boldsymbol{\phi} = [\phi_1, \cdots, \phi_N]$ as the phase shifts of the reflecting coefficients. It should be noted that the RIS cannot be deployed arbitrarily. As a result, the coordinate of RIS $\boldsymbol{l} = [x, y, z]$ has the following constraints as

$$C5: \boldsymbol{l} \in \mathcal{A}_{RIS}, \tag{30}$$

where $\mathcal{A}_{RIS}$ denotes the feasible area that the RIS can be installed. Note that constraints (30) are imposed on each dimension separately. For instance, a possible constant for the height z is $Z_{min} < z < Z_{max}$, where Z_{min} and Z_{max} respectively denote the minimum and maximum installation heights on the Z axis. Thus, constraints (30) are convex with respect to $\boldsymbol{l}$.

It is observed that the sum rate of IUs and the harvested power for EUs depend on the coordinate of RIS, the transmit precoding matrices and the reflecting coefficients of the RIS. Then, we can formulate the problem as:

$$\begin{aligned}\max_{\boldsymbol{\beta},\boldsymbol{\phi},\boldsymbol{l},\boldsymbol{F}_{k,i}} \quad & R_s = \sum_{k=1}^{K}\sum_{i=1}^{I}R_{k,i} \\ \text{s.t.} \quad & C1 - C5.\end{aligned} \tag{31}$$

It can be seen that Problem (31) is a non-convex optimization problem due to the following reasons. First of all, the optimization variables are coupled together and the objective function is intractable. Moreover, according to the RIS-assisted channel model in Section II-B, there is a complicated relationship between the position of RIS, the RIS's reflecting coefficients and the channel gain. Therefore, effective reformulation and simplification are required to tackle the above non-convex optimization problem.

III. Solution Analysis

The original Problem (31) is non-convex and challenging to solve, we first reformulate the problem by leveraging the equivalence between the minimum mean-square error (MMSE) and the signal-to-interference-plus-noise ratio (SINR) . At IU i, the receive decoding matrix $\boldsymbol{U}_{k,i} \in \mathbb{C}^{N_r\times d}$ is applied to the received signal on SB k so that $\hat{\boldsymbol{s}}_{k,i} = \boldsymbol{U}_{k,i}^H\boldsymbol{y}_{k,i}$.

This article has been accepted for publication in a future issue of this journal, but has not been fully edited. Content may change prior to final publication. Citation information: DOI10.1109/TWC.2022.3140268, IEEE Transactions on Wireless Communications

Then, the received mean square error (MSE) of IU i on SB k is given by

$$\begin{aligned}\boldsymbol{E}_{k,i} &= \mathbb{E}_{\boldsymbol{s},\boldsymbol{n}}\left[(\hat{\boldsymbol{s}}_{k,i}-\boldsymbol{s}_{k,i})(\hat{\boldsymbol{s}}_{k,i}-\boldsymbol{s}_{k,i})^H\right] \\ &= (\boldsymbol{U}_{k,i}^H\boldsymbol{Z}_{k,i}\boldsymbol{F}_{k,i}-\boldsymbol{I}_d)^2+\sum_{u\neq i}^{I}\boldsymbol{U}_{k,i}^H\boldsymbol{Z}_{k,i}\boldsymbol{F}_{k,u}\boldsymbol{F}_{k,u}^H\boldsymbol{Z}_{k,i}^H\boldsymbol{U}_{k,i} \\ &\quad+\boldsymbol{U}_{k,i}^2\sigma_{k,i}^2. \end{aligned} \tag{32}$$

The optimal MMSE decoding matrix $\{\boldsymbol{U}_{k,i}\}$ is given by

$$\boldsymbol{U}_{k,i}=(\boldsymbol{Z}_{k,i}\boldsymbol{F}_{k,i}\boldsymbol{F}_{k,i}^H\boldsymbol{Z}_{k,i}^H+\boldsymbol{J}_{k,i})^{-1}\boldsymbol{Z}_{k,i}\boldsymbol{F}_{k,i}. \tag{33}$$

Then, substituting (33) into (32), we have

$$\boldsymbol{E}_{k,i}^{\min}=\boldsymbol{I}_d-\boldsymbol{F}_{k,i}^H\boldsymbol{Z}_{k,i}^H(\boldsymbol{Z}_{k,i}\boldsymbol{F}_{k,i}\boldsymbol{F}_{k,i}^H\boldsymbol{Z}_{k,i}^H+\boldsymbol{J}_{k,i})^{-1}\boldsymbol{Z}_{k,i}\boldsymbol{F}_{k,i}. \tag{34}$$

According to the relationship between the $\boldsymbol{E}_{k,i}^{\min}$ and the SINR shown in [52], the original Problem (31) can be reformulated as Problem (35) by introducing a set of auxiliary variables $\{\boldsymbol{W}_{k,i}\}$ together with the receiving matrices $\{\boldsymbol{U}_{k,i}\}$.

$$\min_{\substack{\boldsymbol{F}_{k,i},\boldsymbol{W}_{k,i},\boldsymbol{U}_{k,i}\\ \boldsymbol{\beta},\boldsymbol{\phi},\boldsymbol{l},}} O^{tot}=\sum_{k=1}^{K}\sum_{i=1}^{I}\left(\mathrm{tr}\left(\boldsymbol{W}_{k,i}\boldsymbol{E}_{k,i}\right)-\log|\boldsymbol{W}_{k,i}|\right) \tag{35a}$$

$$\text{s.t.}\quad \boldsymbol{W}_{k,i}\succ 0,\forall k,i, \tag{35b}$$

$$C1-C4, \tag{35c}$$

where constraints (35b) are imposed for the positive definite matrix $\{\boldsymbol{W}_{k,i}\}$.

Although Problem (35) has more optimization variables, the objective function of Problem (35) is more tractable. Consequently, Problem (35) can be solved by employing the BCD algorithm, where the optimization variables can be iteratively obtained while keeping the others fixed. That is to say, we decouple the optimization problem into three subproblems: optimization of the precoding for IUs, RIS's reflecting coefficients and RIS's coordinate. Note that the receiving matrices $\{\boldsymbol{U}_{k,i}\}$ and the auxiliary matrices $\boldsymbol{W}_{k,i}$ can be directly solved according to the above analysis. Then, the optimal decoding matrix $\{\boldsymbol{U}_{k,i}\}$ is given by (33), and the optimal $\boldsymbol{W}_{k,i}^*$ is given by

$$\boldsymbol{W}_{k,i}^*=(\boldsymbol{E}_{k,i}^{\min})^{-1}. \tag{36}$$

The equivalence between Problem (31) and Problem (35) can be verified by substituting $\boldsymbol{W}_{k,i}^*$, (34) into (35a) and utilizing the matrix inversion lemma, i.e $(\boldsymbol{A}+\boldsymbol{BCD})^{-1}=\boldsymbol{A}^{-1}-\boldsymbol{A}^{-1}\boldsymbol{B}(\boldsymbol{DA}^{-1}\boldsymbol{B}+\boldsymbol{C}^{-1})^{-1}\boldsymbol{DA}^{-1}$ and $|\boldsymbol{I}+\boldsymbol{AB}|=|\boldsymbol{I}+\boldsymbol{BA}|$.

A. Precoding Matrices Design

Given the coordinate of RIS $\boldsymbol{l}$, RIS's reflecting coefficients, auxiliary matrices $\boldsymbol{W}_{k,i}$ and $\{\boldsymbol{U}_{k,i}\}$, the precoding matrices are optimized in this section. By substituting the MSE $\boldsymbol{E}_{k,i}$ in (32) into (35) and discarding the constant terms, the precoding matrices $\boldsymbol{F}_{k,i}$ are determined by the following problem

$$\begin{aligned}&\min_{\boldsymbol{F}_{k,i}}\sum_{k=1}^{K}\sum_{i=1}^{I}\mathrm{tr}\left(\boldsymbol{F}_{k,i}^H\bar{\boldsymbol{W}}_k\boldsymbol{F}_{k,i}\right)-\sum_{k=1}^{K}\sum_{i=1}^{I}2\Re\left[\mathrm{tr}(\bar{\boldsymbol{Z}}_{k,i}\boldsymbol{F}_{k,i})\right]\\ &\text{s.t.}\quad C2-C4,\end{aligned} \tag{37}$$

where $\bar{\boldsymbol{W}}_k=\sum_{i=1}^{I}\boldsymbol{Z}_{k,i}^H\boldsymbol{U}_{k,i}\boldsymbol{W}_{k,i}\boldsymbol{U}_{k,i}^H\boldsymbol{Z}_{k,i}$ and $\bar{\boldsymbol{Z}}_{k,i}=\boldsymbol{W}_{k,i}\boldsymbol{U}_{k,i}^H\boldsymbol{Z}_{k,i}$. Although the objective function of Problem (37) is convex, the energy harvesting constraints $C3$ and $C4$ are non-convex. Note that $\boldsymbol{I}-\boldsymbol{\Phi}_n^H\boldsymbol{\Phi}_n$ is positive definite. As a result, we adopt the successive convex approximation method by leveraging the first-order Taylor expansions with the given precoding matrix $\bar{\boldsymbol{F}}_{k,i}$ as

$$\mathrm{tr}(\boldsymbol{F}_{k,i}^H\boldsymbol{B}_k\boldsymbol{F}_{k,i})\geq 2\Re\{\mathrm{tr}(\bar{\boldsymbol{F}}_{k,i}^H\boldsymbol{B}_k\boldsymbol{F}_{k,i})\}-\mathrm{tr}(\bar{\boldsymbol{F}}_{k,i}^H\boldsymbol{B}_k\bar{\boldsymbol{F}}_{k,i}), \tag{38}$$

$$\mathrm{tr}(\boldsymbol{F}_{k,i}^H\boldsymbol{C}_{k,m}\boldsymbol{F}_{k,i})\geq 2\Re\{\mathrm{tr}(\bar{\boldsymbol{F}}_{k,i}^H\boldsymbol{C}_{k,m}\boldsymbol{F}_{k,i})\}-\mathrm{tr}(\bar{\boldsymbol{F}}_{k,i}^H\boldsymbol{C}_{k,m}\bar{\boldsymbol{F}}_{k,i}), \tag{39}$$

where $\boldsymbol{B}_k=\eta_k\boldsymbol{H}_k^H(\boldsymbol{I}-\boldsymbol{\Phi}^H\boldsymbol{\Phi})\boldsymbol{H}_k$ and $\boldsymbol{C}_{k,m}=\eta_k\boldsymbol{Z}_{k,m}^H\boldsymbol{Z}_{k,m}$. Then, $C3$ and $C4$ can be respectively reformulated as

$$\sum_{k=1}^{K}\sum_{i=1}^{I}2\Re\{\mathrm{tr}(\bar{\boldsymbol{F}}_{k,i}^H\boldsymbol{B}_k\boldsymbol{F}_{k,i})\}\geq\sum_{k=1}^{K}\sum_{i=1}^{I}\mathrm{tr}(\bar{\boldsymbol{F}}_{k,i}^H\boldsymbol{B}_k\bar{\boldsymbol{F}}_{k,i})+P_{RIS}, \tag{40}$$

$$\sum_{k=1}^{K}\sum_{i=1}^{I}2\Re\{\mathrm{tr}(\bar{\boldsymbol{F}}_{k,i}^H\boldsymbol{C}_{k,m}\boldsymbol{F}_{k,i})\}\geq\sum_{k=1}^{K}\sum_{i=1}^{I}\mathrm{tr}(\bar{\boldsymbol{F}}_{k,i}^H\boldsymbol{C}_{k,m}\bar{\boldsymbol{F}}_{k,i})+P_m^{UE}. \tag{41}$$

Then, by replacing $C3$ and $C4$ with (40) and (41) respectively, Problem (37) can be transformed into a series of convex problems, which can be solved by standard tools, such as the CVX.

B. RIS Reflecting Coefficient Optimization

Given $\{\boldsymbol{W}_{k,i}\}$, $\{\boldsymbol{U}_{k,i}\}$, $\{\boldsymbol{F}_{k,i}\}$ and the RIS's coordinate $\boldsymbol{l}$, we consider the optimization of RIS's reflecting coefficients $\varphi_n=\beta_n\exp(j\phi_n)$, where the reflecting phase shift matrix is $\boldsymbol{\Phi}=\mathrm{diag}\{[\varphi_n]_{n=1}^N\}$.

According to the MSE given in (32), we have

$$\begin{aligned}\mathrm{tr}(\boldsymbol{W}_{k,i}\boldsymbol{E}_{k,i})&=\mathrm{tr}(\boldsymbol{W}_{k,i}\boldsymbol{U}_{k,i}^H\boldsymbol{Z}_{k,i}\boldsymbol{F}_k^s\boldsymbol{Z}_{k,i}^H\boldsymbol{U}_{k,i})\\ &\quad-2\Re\left[\mathrm{tr}(\boldsymbol{Z}_{k,i}\boldsymbol{F}_{k,i}\boldsymbol{W}_{k,i}\boldsymbol{U}_{k,i}^H)\right]+\mathrm{const},\end{aligned} \tag{42}$$

where $\boldsymbol{F}_k^s=\sum_{u=1}^{I}\boldsymbol{F}_{k,u}\boldsymbol{F}_{k,u}^H$. The term "const" denotes the constant that is irrelevant with the reflecting coefficients φ_n. As $\boldsymbol{Z}_{k,i}=\boldsymbol{H}_{k,i}+\boldsymbol{G}_{k,i}$, by removing the irrelevant terms in (42), the reflecting coefficient optimization problem is formulated as

$$\begin{aligned}&\min_{\boldsymbol{\varphi}}\sum_{k=1}^{K}\sum_{i=1}^{I}O_{k,i}(\boldsymbol{\varphi})\\ &\text{s.t.}\quad C1,C3,C4,\end{aligned} \tag{43}$$

where $\boldsymbol{\varphi}=[\varphi_1,\cdots,\varphi_N]^T$. In the objective function of (43), for simplicity, we define $\bar{\boldsymbol{U}}_{k,i}=\boldsymbol{U}_{k,i}\boldsymbol{W}_{k,i}\boldsymbol{U}_{k,i}^H$, $\bar{\boldsymbol{F}}_{k,i}=\boldsymbol{F}_{k,i}\boldsymbol{W}_{k,i}\boldsymbol{U}_{k,i}^H$, and then we have

$$\begin{aligned}O_{k,i}(\boldsymbol{\varphi})&=2\Re[\mathrm{tr}(\boldsymbol{G}_{k,i}\boldsymbol{F}_k^s\boldsymbol{H}_{k,i}^H\bar{\boldsymbol{U}}_{k,i})]+\mathrm{tr}(\boldsymbol{G}_{k,i}\boldsymbol{F}_k^s\boldsymbol{G}_{k,i}^H\bar{\boldsymbol{U}}_{k,i})\\ &\quad-2\Re[\mathrm{tr}(\boldsymbol{G}_{k,i}\bar{\boldsymbol{F}}_{k,i})].\end{aligned} \tag{44}$$

Note that $\bar{\boldsymbol{U}}_{k,i}$ is hermitian, but it is still difficult to solve Problem (43) with this formulation.

To obtain a more tractable problem formulation, we define $\boldsymbol{u}_{k,i} = \boldsymbol{e}_{k,i}^H \odot \boldsymbol{e}_k^T$. Then, the RIS assisted channel gain is represented as

$$\boldsymbol{G}_{k,i} = g_{k,i}(\boldsymbol{u}_{k,i}\boldsymbol{\varphi})\boldsymbol{r}_{k,i}\boldsymbol{v}_k^H. \tag{45}$$

Substituting (45) into (44), we have

$$O_{k,i}(\boldsymbol{\varphi}) = 2\Re\{g_{k,i}\xi_{k,i}\boldsymbol{u}_{k,i}\boldsymbol{\varphi}\} + A_{k,i}|g_{k,i}|^2|\boldsymbol{u}_{k,i}\boldsymbol{\varphi}|^2, \tag{46}$$

where $A_{k,i} = \text{tr}(\boldsymbol{r}_{k,i}\boldsymbol{v}_k^H\boldsymbol{F}_k^s\boldsymbol{v}_k\boldsymbol{r}_{k,i}^H\bar{\boldsymbol{U}}_{k,i})$, and $\xi_{k,i} = (\text{tr}(\boldsymbol{r}_{k,i}\boldsymbol{v}_k^H\boldsymbol{F}_k^s\boldsymbol{H}_{k,i}^H\bar{\boldsymbol{U}}_{k,i}) - \text{tr}(\boldsymbol{r}_{k,i}\boldsymbol{v}_k^H\bar{\boldsymbol{F}}_{k,i}))$.

Similarly, according to (12), constraint $C3$ can be reformulated as

$$\begin{aligned}&\text{tr}\left(\boldsymbol{F}_{k,i}^H\boldsymbol{H}_k^H(\boldsymbol{I}-\boldsymbol{\Phi}^H\boldsymbol{\Phi})\boldsymbol{H}_k\boldsymbol{F}_{k,i}\right)\\&\quad= |H_k|^2\text{tr}\left(\boldsymbol{F}_{k,i}^H\boldsymbol{v}_k\boldsymbol{v}_k^H\boldsymbol{F}_{k,i}\right)(N-\boldsymbol{\varphi}^H\boldsymbol{\varphi}),\end{aligned} \tag{47}$$

where the LOS channel $\boldsymbol{H}_k = H_k\boldsymbol{e}_k\boldsymbol{v}_k^H$ and $\boldsymbol{e}_k^H\boldsymbol{e}_k = N$ are utilized to obtain the right hand side. Also, the complex channel gain H_k is given in (11).

Similarly, for constraint $C4$, by substituting $\boldsymbol{Z}_{k,m} = \boldsymbol{H}_{k,m} + \boldsymbol{G}_{k,m}$ and (45) into $C4$, we have the following reformulation as

$$\begin{aligned}\sum_{i=1}^{I}\text{tr}\left(\boldsymbol{Z}_{k,m}\boldsymbol{F}_{k,i}\boldsymbol{F}_{k,i}^H\boldsymbol{Z}_{k,m}^H\right) &= |g_{k,m}|^2\Lambda_{k,m}(\boldsymbol{u}_{k,m}\boldsymbol{\varphi})^2\\&\quad+2\Re\{g_{k,m}w_{k,m}\boldsymbol{u}_{k,m}\boldsymbol{\varphi}\}+Q_{k,m},\end{aligned} \tag{48}$$

where $\Lambda_{k,m} = \text{tr}\left(\boldsymbol{r}_{k,i}\boldsymbol{v}_k^H\boldsymbol{F}_k^s\boldsymbol{v}_k\boldsymbol{r}_{k,i}^H\right)$, $w_{k,m} = \text{tr}\left(\boldsymbol{r}_{k,i}\boldsymbol{v}_k^H\boldsymbol{F}_k^s\boldsymbol{H}_{k,m}^H\right)$, and $Q_{k,m} = \text{tr}\left(\boldsymbol{H}_{k,m}\boldsymbol{F}_k^s\boldsymbol{H}_{k,m}^H\right)$.

According to (45), (47) and (48), the RIS's reflecting coefficient problem can be reformulated as

$$\min_{\boldsymbol{\varphi}} \quad \boldsymbol{\varphi}^H\boldsymbol{A}\boldsymbol{\varphi} + \Re\{\boldsymbol{\xi}\boldsymbol{\varphi}\} \tag{49a}$$

$$\text{s.t.} \quad \boldsymbol{\varphi}^H\boldsymbol{\Lambda}_m\boldsymbol{\varphi} + \Re\{\boldsymbol{\omega}_m\boldsymbol{\varphi}\} \geq \tilde{P}_m^U. \tag{49b}$$

$$(N-\boldsymbol{\varphi}^H\boldsymbol{\varphi})C_{RIS} \geq P^I \tag{49c}$$

$$|\boldsymbol{\varphi}| \leq \mathbf{1}. \tag{49d}$$

where

$$\boldsymbol{A} = \sum_{k=1}^{K}\sum_{i=1}^{I}A_{k,i}|g_{k,i}|^2\boldsymbol{u}_{k,i}^H\boldsymbol{u}_{k,i},\ \boldsymbol{\xi} = \sum_{k=1}^{K}\sum_{i=1}^{I}2g_{k,i}\xi_{k,i}\boldsymbol{u}_{k,i},$$

$$\boldsymbol{\Lambda}_m = \sum_{k=1}^{K}\eta_k|g_{k,m}|^2\Lambda_{k,m}\boldsymbol{u}_{k,m}^H\boldsymbol{u}_{k,m},$$

$$\boldsymbol{\omega}_m = 2\sum_{k=1}^{K}\eta_k g_{k,m}w_{k,m}\boldsymbol{u}_{k,m},$$

$$\tilde{P}_m^U = P_m^U - \sum_{k=1}^{K}Q_{k,m}, \text{and}$$

$$C_{RIS} = \sum_{k=1}^{K}\sum_{i=1}^{I}\eta_k(H_k)^2\text{tr}\left(\boldsymbol{F}_{k,i}^H\boldsymbol{v}_k\boldsymbol{v}_k^H\boldsymbol{F}_{k,i}\right).$$

However, it is observed that constraint (49b) is non-convex. Note that $\boldsymbol{\Lambda}_m$ is positive-definite so that we adopt the first-order Taylor expansion for convex approximation. At given $\bar{\boldsymbol{\varphi}}$, we have

$$\boldsymbol{\varphi}^H\boldsymbol{\Lambda}_m\boldsymbol{\varphi} \geq 2\Re\{\boldsymbol{\varphi}^H\boldsymbol{\Lambda}_m\bar{\boldsymbol{\varphi}}\} - \bar{\boldsymbol{\varphi}}^H\boldsymbol{\Lambda}_m\bar{\boldsymbol{\varphi}}. \tag{50}$$

By utilizing (50) to simplify (49b), Problem (49) can be transformed into a series of simple convex problems, which can be easily solved by CVX.

C. Optimization of RIS's Coordinate

We consider the optimization of RIS coordinate with given $\boldsymbol{W}_{k,i}$ and $\{\boldsymbol{U}_{k,i}\}$, $\{\boldsymbol{F}_{k,i}\}$ and the phase shift matrix $\boldsymbol{\Phi}$. In this case, based on the formulations given in (46), (47) and (48), the original Problem (35) is formulated as

$$\begin{aligned}\min_{\boldsymbol{l}} \quad & O^{tot}(\boldsymbol{l}) = \sum_{k=1}^{K}\sum_{i=1}^{I}|g_{k,i}(\boldsymbol{l})|^2E_{k,i}(\boldsymbol{l}) +\\&\quad \Re\{g_{k,i}(\boldsymbol{l})F_{k,i}(\boldsymbol{l})\} + Cst(\boldsymbol{W}_{k,i},\boldsymbol{U}_{k,i},\boldsymbol{F}_{k,i})\end{aligned} \tag{51a}$$

$$\begin{aligned}\text{s.t.} \quad & \sum_{k=1}^{K}(|g_{k,m}(\boldsymbol{l})|^2\lambda_{k,m}(\boldsymbol{l}) + \Re\{g_{k,m}(\boldsymbol{l})\chi_{k,m}(\boldsymbol{l})\}\\&\quad + \eta_k Q_{k,m}) \geq P_m^U,\end{aligned} \tag{51b}$$

$$\sum_{k=1}^{K}|H_k(\boldsymbol{l})|^2D_k(\boldsymbol{l}) \geq P^I, \tag{51c}$$

where $Cst(\boldsymbol{W}_{k,i},\boldsymbol{U}_{k,i},\boldsymbol{F}_{k,i})$ is the constant term, and

$$E_{k,i}(\boldsymbol{l}) = A_{k,i}(\boldsymbol{l})|\boldsymbol{u}_{k,i}(\boldsymbol{l})\boldsymbol{\varphi}|^2, \tag{52}$$

$$F_{k,i}(\boldsymbol{l}) = 2\xi_{k,i}(\boldsymbol{l})\boldsymbol{u}_{k,i}(\boldsymbol{l})\boldsymbol{\varphi}, \tag{53}$$

$$\lambda_{k,m}(\boldsymbol{l}) = \eta_k\Lambda_{k,m}(\boldsymbol{l})|\boldsymbol{u}_{k,m}(\boldsymbol{l})\boldsymbol{\varphi}|^2, \tag{54}$$

$$\chi_{k,m}(\boldsymbol{l}) = 2\eta_k w_{k,m}(\boldsymbol{l})\boldsymbol{u}_{k,m}(\boldsymbol{l})\boldsymbol{\varphi}, \tag{55}$$

$$D_k(\boldsymbol{l}) = \sum_{i=1}^{I}\eta_k\text{tr}\left(\boldsymbol{F}_{k,i}^H\boldsymbol{v}_k(\boldsymbol{l})\boldsymbol{v}_k^H(\boldsymbol{l})\boldsymbol{F}_{k,i}\right)(N-\boldsymbol{\varphi}^H\boldsymbol{\varphi}). \tag{56}$$

According to the channel model, many periodic cosine components with respect to the SB's index and UE's index are involved in $E_{k,i}(\boldsymbol{l})$, $F_{k,i}(\boldsymbol{l})$, $\lambda_{k,m}(\boldsymbol{l})$, $\chi_{k,m}(\boldsymbol{l})$ and $D_k(\boldsymbol{l})$. However, they are all dependent on the RIS's coordinate $\boldsymbol{l} = [X,Y,Z]^T$. Their complex expressions make it very difficult to directly optimize the objective function given in (51a).

However, given the initial RIS's coordinate $\boldsymbol{l}^{(0)} = [X,Y,Z]^T$, the values of (52)-(56) can be calculated as $E_{k,i}(\boldsymbol{l}^{(0)}), F_{k,i}(\boldsymbol{l}^{(0)}), \lambda_{k,m}(\boldsymbol{l}^{(0)}), \chi_{k,m}(\boldsymbol{l}^{(0)}), D_k(\boldsymbol{l}^{(0)})$, respectively. Consequently, if we replace (52)-(56) with the constants evaluated by a given location, for instance, replace $E_{k,i}(\boldsymbol{l})$ with $E_{k,i}(\boldsymbol{l}^{(0)})$, Problem (51) can be simplified into a tractable formulation.

First of all, for ease of exposition, we define auxiliary variables r_u and d_0, which are dependent on the RIS's coordinate $\boldsymbol{l}$ by

$$d_0 = |\boldsymbol{l}-\boldsymbol{s}_{AP}|, r_u = |\boldsymbol{l}-\boldsymbol{s}_u|, u \in \mathcal{I}\cup\mathcal{M}. \tag{57}$$

Then, we define the function $f_{k,u}(r_u,d_0)$ with respect to (r_u,d_0) as

$$f_{k,u}(r_u,d_0) = \frac{\mu_k}{r_u d_0}\exp\left(-K_k(r_u+d_0)\right), u \in \mathcal{I}\cup\mathcal{M}, \tag{58}$$

where $\mu_k = \frac{G_t G_r\lambda_k}{8\sqrt{\pi^3}}$, and $K_k = \frac{K(f_k)}{2}$.

According to (19), the cascaded channel gain $g_{k,i}(\boldsymbol{l})$ can be represented as a function with respect to (r_i, d_0) as

$$g_{k,i}(r_i, d_0) = f_{k,i}(r_i, d_0) \exp\left(-j2\pi \frac{r_i + d_0}{\lambda_k}\right), u \in \mathcal{I} \cup \mathcal{M}. \tag{59}$$

Then, we have the conclusion that $f_{k,u}(r_u, d_0)$ and $f^2_{k,u}(r_u, d_0)$ are all convex with respect to (r_u, d_0). The proof can be found in Appendix A.

Next, the simplifications of the objective function and constraints are investigated to help find the tractable formulation of Problem (51).

1) Simplification of Objective Function: As the solution is obtained by the iterative algorithm, we denote a RIS's coordinate obtained at the n-th iteration as $\boldsymbol{l}^{(n)}$. To simplify objective function (51a), substituting $\boldsymbol{l}^{(n)}$ into (52) and (53), we can obtain the following *constants* as

$$E_{k,i} \triangleq E_{k,i}(\boldsymbol{l}^{(n)}),$$
$$F_{k,i} \triangleq \Re\left\{\exp\left(-j2\pi \frac{\tilde{r}_i + \tilde{d}_0}{\lambda_k}\right) F_{k,i}(\boldsymbol{l}^{(n)})\right\}, i \in \mathcal{I},$$

where *constants* $\tilde{r}_i$ and $\tilde{d}_0$ are obtained by leveraging $\boldsymbol{l}^{(n)}$ as $\tilde{r}_i = |\boldsymbol{l}^{(n)} - \boldsymbol{s}_i^1|, \tilde{d}_0 = |\boldsymbol{l}^{(n)} - \boldsymbol{s}_{AP}^1|$.

Then, it is observed that *constants* $E_{k,i}$ are always positive according to (52). However, note that the calculated coefficient $F_{k,i}$ is not necessarily positive. Consequently, as $f_{k,i}(r_i, d_0)$is convex, its first-order Taylor expansion of $f_{k,i}(r_i, d_0)$ is adopted for simplification as

$$f_{k,i}(r_i, d_0) \geq f_{k,i}(\tilde{r}_i, \tilde{d}_0) + \nabla_{r_i} f_{k,i}(\tilde{r}_i, \tilde{d}_0)(r_i - \tilde{r}_i) + \nabla_{d_0} f_{k,i}(\tilde{r}_i, \tilde{d}_0)(d_0 - \tilde{d}_0), \tag{60}$$

where the first-order derivative is defined as

$$\nabla_x f_{k,i}(x, y) = -\mu_k \frac{K_k x + 1}{x^2 y} \exp\left(-K_k(x + y)\right). \tag{61}$$

Consequently, by leveraging the calculated $E_{k,i}$, $F_{k,i}$ and discarding the irrelevant constants, a simplified version of the objective function (51a) is given by

$$O_{\boldsymbol{l}^{(n)}}(r_i, d_0) = \sum_{k=1}^{K}\sum_{i=1}^{I}(f^2_{k,i}(r_i, d_0)E_{k,i} + F_{k,i}(\nabla_{r_i} f_{k,i}(\tilde{r}_i, \tilde{d}_0)r_i + \nabla_{d_0} f_{k,i}(\tilde{r}_i, \tilde{d}_0)d_0)). \tag{62}$$

It is observed that the objective function $O_{\boldsymbol{l}^{(n)}}(r_i, d_0)$ is convex with respect to (r_i, d_0).

2) Simplified EUs Constraints: Then, we deal with constraint (51b) for EU m.

By substituting coordinate $\boldsymbol{l}^{(n)}$ into (54) and (55), the following *constants* can be obtained as

$$\lambda_{k,m} \triangleq \lambda_{k,m}(\boldsymbol{l}^{(n)}),$$
$$\chi_{k,m} \triangleq \Re\left\{\exp\left(-j2\pi \frac{\tilde{r}_m + \tilde{d}_0}{\lambda_k}\right) \chi_{k,m}(\boldsymbol{l}^{(n)})\right\}, m \in \mathcal{M},$$

where the constant $\tilde{r}_m = |\boldsymbol{l}^{(n)} - \boldsymbol{s}_m|$ is calculated with coordinate $\boldsymbol{l}^{(n)}$.

Then, by employing the function $f_{k,m}(r_m, d_0), m \in \mathcal{M}$ in (58), the constants $\lambda_{k,m}$ and $\chi_{k,m}$, constraint (51b) is rewritten as

$$\sum_{k=1}^{K}(f^2_{k,m}(r_m, d_0)\lambda_{k,m} + f_{k,m}(r_u, d_0)\chi_{k,m} + \eta_k Q_{k,m}) \geq P_m^U, m \in \mathcal{M}. \tag{63}$$

However, (63) is still non-convex. As $f_{k,m}(r_u, d_0)$ and $f^2_{k,m}(r_u, d_0)$ are both convex functions as proved in Appendix A, their first-order Taylor expansions are

$$f^2_{k,m}(r_m, d_0) \geq f^2_{k,m}(\tilde{r}_m, \tilde{d}_0) + \nabla_{r_m} f^2_{k,m}(\tilde{r}_m, \tilde{d}_0)(r_m - \tilde{r}_m) + \nabla_{d_0} f^2_{k,m}(\tilde{r}_m, \tilde{d}_0)(d_0 - \tilde{d}_0), \tag{64}$$

$$f_{k,m}(r_m, d_0) \geq f_{k,i}(\tilde{r}_m, \tilde{d}_0) + \nabla_{r_m} f_{k,m}(\tilde{r}_i, \tilde{d}_0)(r_m - \tilde{r}_m) + \nabla_{d_0} f_{k,m}(\tilde{r}_m, \tilde{d}_0)(d_0 - \tilde{d}_0), \tag{65}$$

where $\nabla_x f_{k,m}(x, y)$ is given in (61), and $\nabla_x f^2_{k,m}(x, y) = 2f_{k,m}(x, y)\nabla_x f_{k,m}(x, y)$.

Then, substituting (64) and (65) into (63), constraint (51b) for EU m can be further reformulated as

$$A_m(\boldsymbol{l}^{(n)}, \tilde{r}_m, \tilde{d}_0)r_m + B_m(\boldsymbol{l}^{(n)}, \tilde{r}_m, \tilde{d}_0)d_0 + C_m(\boldsymbol{l}^{(n)}, \tilde{r}_m, \tilde{d}_0) \geq P_m^U, m \in \mathcal{M}, \tag{66}$$

where$A_m(\boldsymbol{l}^{(n)}, \tilde{r}_m, \tilde{d}_0) = \sum_{k=1}^{K}\Big(\lambda_{k,m}(\boldsymbol{l}^{(n)})\nabla_{r_m} f^2_{k,m}(\tilde{r}_m, \tilde{d}_0) + \chi_{k,m}(\boldsymbol{l}^{(n)})\nabla_{r_m} f_{k,m}(\tilde{r}_m, \tilde{d}_0)\Big)$, $B_m(\boldsymbol{l}^{(n)}, \tilde{r}_m, \tilde{d}_0) = \sum_{k=1}^{K}\Big(\lambda_{k,m}(\boldsymbol{l}^{(n)})\nabla_{d_0} f^2_{k,m}(\tilde{r}_m, \tilde{d}_0) + \chi_{k,m}(\boldsymbol{l}^{(n)})\nabla_{d_0} f_{k,m}(\tilde{r}_m, \tilde{d}_0)\Big)$, and $C_m(\boldsymbol{l}^{(n)}, \tilde{r}_m, \tilde{d}_0) = \sum_{k=1}^{K}(\lambda_{k,m}(\boldsymbol{l}^{(n)})f^2_{k,m}(\tilde{r}_m, \tilde{d}_0) + \chi_{k,m}(\boldsymbol{l}^{(n)})f_{k,m}(\tilde{r}_m, \tilde{d}_0)) - A_m(\boldsymbol{l}^{(n)}, \tilde{r}_m, \tilde{d}_0)\tilde{r}_m - B_m(\boldsymbol{l}^{(n)}, \tilde{r}_m, \tilde{d}_0)\tilde{d}_0 + \sum_{k=1}^{K}\eta_k Q_{k,m}$.

3) Simplification of Constraints for RIS: Similarly, constraint (51c) for the RIS is simplified in the following. We first define function $h_k(d_0)$ as

$$h_k(d_0) = \frac{\rho_k}{d_0^2} \exp\left(-2K_k d_0\right), \tag{67}$$

where $\rho_k = \left(\frac{\lambda_k}{4\pi}\right)^2$. By checking the Hessian matrix of $h_k(d_0)$, it can be verified that $h_k(d_0)$ is convex with respect to d_0. Also, by substituting the coordinate $\boldsymbol{l}^{(n)}$ into (56), *constants* D_k can be obtained as $D_k \triangleq D_k(\boldsymbol{l}^{(n)})$.

However, by employing the function $h_k(d_0)$ in (67), and substituting D_k into (51b), the following constraint is still non-convex:

$$\sum_{k=1}^{K} h_k(d_0)D_k \geq P^I. \tag{68}$$

Therefore, the first-order Taylor expansion of $h_k(d_0)$ is utilized for convex approximation,

$$h_k(d_0) \geq h_k(\tilde{d}_0) + \nabla_{d_0}^{h_k}(\tilde{d}_0)(d_0 - \tilde{d}_0), \tag{69}$$

where $\nabla_{d_0}^{h_k}(\tilde{d}_0)$ represents the first-order derivative of $h_k(d_0)$ given by

$$\nabla_{d_0}^{h_k}(d_0) = -\rho_k \frac{2K_k d_0 + 2}{d_0^3} \exp\left(-2K_k d_0\right).$$

This article has been accepted for publication in a future issue of this journal, but has not been fully edited. Content may change prior to final publication. Citation information: DOI10.1109/TWC.2022.3140268, IEEE Transactions on Wireless Communications

Then, substituting (69) into (51c), we have

$$A_{RIS}(\boldsymbol{l}^{(n)}, \tilde{d}_0)d_0 + B_{RIS}(\boldsymbol{l}^{(n)}, \tilde{d}_0) \geq P^I, \tag{70}$$

where the constants are evaluated as

$$A_{RIS}(\boldsymbol{l}^{(n)}, \tilde{d}_0) = \sum_{k=1}^{K} D_k(\boldsymbol{l}^{(n)}) \nabla_{d_0}^{h_k}(\tilde{d}_0), \tag{71}$$

$$B_{RIS}(\boldsymbol{l}^{(n)}, \tilde{d}_0) = \sum_{k=1}^{K} D_k(\boldsymbol{l}^{(n)}) (h_k(\tilde{d}_0) - \tilde{d}_0 \nabla_{d_0}^{h_k}(\tilde{d}_0)). \tag{72}$$

4) Simplification of Problem (51): Finally, given RIS's coordinate obtained at the n-th iteration denoted as $\boldsymbol{l}^{(n)}$, by replacing $O^{tot}(\boldsymbol{l})$ with $O_{\boldsymbol{l}^{(n)}}(r_i, d_0)$ in (62), replacing (51b) and (51c) with (66) and (70) respectively, Problem (51) is reformulated as

$$\min_{\boldsymbol{l}, r_u, d_0} \quad O_{\boldsymbol{l}^{(n)}}(r_i, d_0) \tag{73a}$$

$$\text{s.t.} \quad |\boldsymbol{l} - \boldsymbol{s}_u^1| \leq r_u, u \in \mathcal{I} \cup \mathcal{M} \tag{73b}$$

$$|\boldsymbol{l} - \boldsymbol{s}_{AP}^1| \leq d_0. \tag{73c}$$

$$(66), (70).$$

Constraints (73b) and (73c) are introduced for the auxiliary variables r_u and d_0. Then, it can be verified that Problem (73) is convex, which can be readily solved by CVX.

However, note that Problem (73) is the simplified version of Problem (51). The optimal solution to Problem (73) denoted by $(\boldsymbol{l}^*, r_u^*, d_0^*)$ may not satisfy all the constraints of Problem (51). Consequently, we need to add the following procedure to ensure that the obtained solution $(\boldsymbol{l}^*, r_u^*, d_0^*)$ is a feasible solution to Problem (51).

5) Feasibility guarantee: First we define the following penalty indicators as

$$\alpha = A_{RIS}(\boldsymbol{l}^*, d_0^*)d_0^* + B_{RIS}(\boldsymbol{l}^*, d_0^*) - P^I, \tag{74}$$

$$\alpha_m = A_m(\boldsymbol{l}^*, r_m^*, d_0^*)r_m^* + B_m(\boldsymbol{l}^*, r_m^*, d_0^*)d_0^* + C_m(\boldsymbol{l}^*, r_m^*, d_0^*) - P_m^U. \tag{75}$$

If $\alpha < 0$, the obtained coordinate $\boldsymbol{l}^*$ does not satisfy constraint (51c). This implies that the distance between RIS and AP is too large, i.e., the power harvested by the RIS does not exceed the requirement. By checking the first-order derivative of $h_k(d_0)$ with respect to d_0 , it is verified that $\nabla_{d_0}^{h_k}(d) < 0, \forall d \geq 0$. According to (71), as $D_k(\boldsymbol{l}^*) \geq 0$ for all coordinates, we have $A_{RIS}(\boldsymbol{l}^*, d_0^*) < 0$. Consequently, to ensure that (51c) is satisfied, the RIS should be closer to the AP, i.e., d_0 should be reduced. To this end, the required harvested power of RIS, i.e., P^I is modified as

$$P^{I'} = P^I + \epsilon, \text{if } \alpha < 0, \tag{76}$$

where $\epsilon > 0$ is the introduced penalty. [1]

Also, if $\alpha_m < 0$, the obtained coordinate $\boldsymbol{l}^*$ does not satisfy constraint (51b) for EU m. Note that $\nabla_x f_{k,m}(x, y) < 0$, $\nabla_y f_{k,m}(x, y) < 0$ and $\lambda_{k,m}(\boldsymbol{l}) \geq 0, \forall \boldsymbol{l}$. Similarly, according to (66), this implies that d_0 or r_m should be decreased to satisfy constraint (51b). Given that d_0 is modified by adjusting P^I, therefore, we only adjust P_m^U to reduce d_m, which should be modified as

$$P_m^{U'} = P_m^U + \epsilon_m, \text{if } \alpha_m < 0, \tag{77}$$

where $\epsilon_m > 0$ is the penalty for EU m.

Overall, constraints (70) and (66) are updated by replacing P^I and P_m^U with $P^{I'}$ and $P_m^{U'}$ in (76) and (77), respectively. The solution to Problem (73) with the modified constraints (70) and (66) should be updated accordingly. Then, the finally obtained solution $(\boldsymbol{l}^*, r_u^*, d_0^*)$ is guaranteed to satisfy all the constraints of Problem (51) when $\alpha \geq 0$ and $\alpha_m \geq 0, \forall m$.

The above analysis can be summarized as the following Penalty Constrained Convex Approximation (PCCA) algorithm shown in Algorithm 1 to optimize the RIS's coordinate. For ease of exposition, the flowchart of PCCA algorithm is provided in Fig. 3.

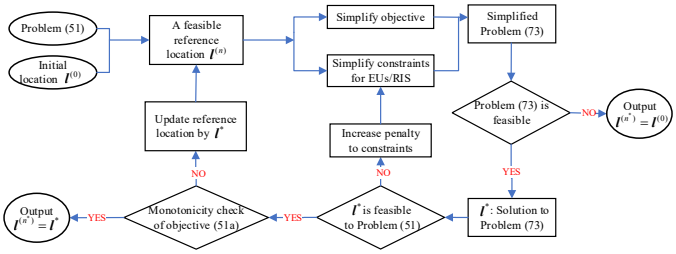

Fig. 3. The flowchart of the PCCA algorithm.

Algorithm 1 Penalty Constrained Convex Approximation Algorithm (PCCA)

1: Initialize coordinate $\boldsymbol{l}^{(0)}$, and the objective $O^{tot}(\boldsymbol{l}^{(0)}, \boldsymbol{W}_{k,i}^0, \boldsymbol{U}_{k,i}^0)$;
2: Initialize iterative number $n = 0$ and maximum number of iterations N_{max};
3: **repeat**
4: Obtain $(\boldsymbol{l}^*, r_u^*, d_0^*)$ by solving Problem (73);
5: **if** $\alpha \geq 0$ and $\alpha_m \geq 0$ **then**
6: Update $\boldsymbol{l}^{n+1} = \boldsymbol{l}^*$;
7: Calculate $\boldsymbol{W}_{k,i}^{n+1}, \boldsymbol{U}_{k,i}^{n+1}$ according to (33) and (36), respectively.
8: Calculate $O^{tot}(\boldsymbol{l}^{n+1}, \boldsymbol{W}_{k,i}^{n+1}, \boldsymbol{U}_{k,i}^{n+1})$;
9: **if** $O^{tot}(\boldsymbol{l}^{n+1}, \boldsymbol{W}_{k,i}^{n+1}, \boldsymbol{U}_{k,i}^{n+1}) < O^{tot}(\boldsymbol{l}^{(0)}, \boldsymbol{W}_{k,i}^0, \boldsymbol{U}_{k,i}^0)$ **then**
10: $\boldsymbol{l}^{(n^*)} = \boldsymbol{l}^{n+1}$;
11: **end if**
12: **else**
13: Update P_m^U for all $m, \alpha_m < 0$ according to (75) ;
14: Update P^I according to (74) if $\alpha < 0$;
15: **if** Problem (73) is not feasible **then**
16: Set $n = N_{max}$ and $\boldsymbol{l}^{(n^*)} = \boldsymbol{l}^0$;
17: **end if**
18: **end if**
19: **until** $n = N_{max}$;
Output: $\boldsymbol{l}^{(n^*)}, \boldsymbol{U}_{k,i}^{n^*}, \boldsymbol{W}_{k,i}^{n^*}$;

Remark 1: Once the obtained $(\boldsymbol{l}^*, r_u^*, d_0^*)$ is a feasible solution to the original Problem (51). We denote it as the

[1] In practice, penalties are set as 1% of the required powers for satisfactory performance, i.e., $\epsilon = 1\% P^I$ and $\epsilon_m = 1\% P_m^U$.

This article has been accepted for publication in a future issue of this journal, but has not been fully edited. Content may change prior to final publication. Citation information: DOI10.1109/TWC.2022.3140268, IEEE Transactions on Wireless Communications

$(n+1)$-th coordinate of the RIS, i.e., $\boldsymbol{l}^{(n+1)} = \boldsymbol{l}^*$ when $\alpha \geq 0$ and $\alpha_m \geq 0, \forall m$. Then, Problem (73) can be formulated based on $\boldsymbol{l}^{(n+1)}$, and the feasible coordinate of RIS for the $(n+2)$-th iteration can be obtained by leveraging the penalties for power harvesting constraints.

Remark 2: In addition, as the objective function $O_{\boldsymbol{l}^{(n)}}(r_i, d_0)$ is the approximation of (51a), we need to check the original objective value $O^{tot}(\boldsymbol{l}^{(n+1)})$ in (51a) at each iteration. Note that the receiver matrix $\boldsymbol{U}_{k,i}^n$ aims to minimize the MSE for a given channel $\boldsymbol{Z}(\boldsymbol{l}^{(n)})$, and weight $\boldsymbol{W}_{k,i}^{(n)}$ depends on the current MMSE matrix. As the channel is optimized by adopting the RIS's new coordinate $\boldsymbol{l}^{(n+1)}$, the receiver matrix $\boldsymbol{U}_{k,i}$ matched to this new channel and the obtained MMSE should be updated according to (33) and (36), respectively. That is to say, the objective value at the $(n+1)$-th iteration is evaluated as $O^{tot}(\boldsymbol{l}^{(n+1)}, \boldsymbol{W}_{k,i}^{n+1}, \boldsymbol{U}_{k,i}^{n+1})$.

Remark 3: We briefly explain the convergence of the PCCA algorithm. According to the flowchart in Fig.3, the output of the PCCA algorithm $\boldsymbol{l}^{(n^*)}$ is either the initial location $\boldsymbol{l}^{(0)}$ (step 16) or the new location $\boldsymbol{l}^*$ (step 10). In the monotonicity check part of PCCA (step 9), the optimized coordinate $\boldsymbol{l}^*$ is compared with the initial coordinate $\boldsymbol{l}^{(0)}$ in terms of the obtained objective value[2]. In this way, only when the objective obtained by $\boldsymbol{l}^*$ decreases, this new location will be selected as the output. Otherwise, PCCA keeps searching next location until Problem (73) becomes infeasible. When Problem (73) is infeasible, PCCA outputs initial location $\boldsymbol{l}^{(0)}$. Consequently, the objective value of PCCA's output is monotonically non-increasing. Also, the area for RIS deployment is limited, so that the value of the objective function is also bounded. As a result, the convergence of the PCCA algorithm is guaranteed.

D. BCD Algorithm to Solve Problem (35)

Based on the above analysis, we propose a BCD based alternating optimization algorithm to solve Problem (35). The BCD algorithm consists of three parts: the precoding design Problem (37) with respect to $\{\boldsymbol{F}_{k,i}\}$, the RIS phase shift optimization Problem (49) with respect to $\{\boldsymbol{\varphi}\}$, and the RIS deployment Problem (51) with respect to $\{\boldsymbol{l}, \boldsymbol{U}_{k,i}, \boldsymbol{W}_{k,i}\}$. These problems are alternately solved with the other optimization variables fixed. The detailed algorithm is presented in Algorithm 2.

In the $(s+1)$-th iteration of the BCD algorithm, Problem (37) and (49) are solved based on the idea of successive convex approximation (SCA). In other words, by successively imposing tight convex restrictions on the constraint sets, the locally tight approximation of the original problems are obtained and solved. The obtained $\boldsymbol{F}_{k,i}^{(s+1)}$ and $\boldsymbol{\varphi}^{(s+1)}$ are the converged result by solving the tight approximated problems successively. Then, it is proved in [53] that $\boldsymbol{F}_{k,i}^{(s+1)}$ and $\boldsymbol{\varphi}^{(s+1)}$ are the KKT points of the original Problem (37) and (49). Consequently, we can infer

$$O^{tot}(\boldsymbol{F}_{k,i}^{(s+1)}, \boldsymbol{\phi}_{k,i}^{(s+1)}, \boldsymbol{l}^{(s)}, \boldsymbol{U}_{k,i}^{(s)}, \boldsymbol{W}_{k,i}^{(s)}) \leq O^{tot}(\boldsymbol{F}_{k,i}^{(s)}, \boldsymbol{\phi}_{k,i}^{(s)}, \boldsymbol{l}^{(s)}, \boldsymbol{U}_{k,i}^{(s)}, \boldsymbol{W}_{k,i}^{(s)}). \quad (78)$$

In addition, according to Remark 3 in Section III-B, the following inequality can be ensured by the PCCA

$$O^{tot}(\boldsymbol{F}_{k,i}^{(s+1)}, \boldsymbol{\phi}_{k,i}^{(s+1)}, \boldsymbol{l}^{(s)}, \boldsymbol{U}_{k,i}^{(s)}, \boldsymbol{W}_{k,i}^{(s)}) \geq O^{tot}(\boldsymbol{F}_{k,i}^{(s+1)}, \boldsymbol{\phi}_{k,i}^{(s+1)}, \boldsymbol{l}^{(s+1)}, \boldsymbol{U}_{k,i}^{(s+1)}, \boldsymbol{W}_{k,i}^{(s+1)}). \quad (79)$$

Combining (78) with (79), it is verified that the objective value obtained by the BCD algorithm is monotonically non-increasing. Also, according to the equivalence between SINR and the MSE, the objective function is bounded as the transmit signal power and signal power are all limited. Thus, the proposed BCD algorithm is guaranteed to converge.

Then, we analyze the complexity of the BCD algorithm. We first analyze the complexity of solving the precoding design Problem (37). Its main complexity lies in solving the convex approximation of Problem (37), which is approximated as a second-order cone program (SOCP) problem. The transformed SOCP problem has $2KIN_td$ real variables, and $M+2$ SOC constraints have $2N_td$ real dimensions. According to [54], the complexity is $\mathcal{O}((2KIN_td)^2(2N_td(M+2)))$, and the number of iterations required is $\mathcal{O}(\sqrt{M+2})$. Also, denote the number of convex approximations for Problem (37) as N_F^{SCA}. Then, the total complexity of solving Problem (37) is $\mathcal{O}(N_F^{SCA}\sqrt{I+K}(2KIN_td)^2(2N_td(M+2)))$.

For the RIS phase shift optimization Problem (49), its approximated convex SOCP problem has $2N$ real variables, and $M+1$ SOC constraints have $2N$ real dimensions. According to [54], the complexity is $\mathcal{O}((2N)^2(2N(M+1)))$, and the number of iterations required is $\mathcal{O}(\sqrt{M+1})$. Denote the number of convex approximations for Problem (37) as N_ϕ^{SCA}. Then, the total complexity of solving Problem (49) is $\mathcal{O}(N_\phi^{SCA}\sqrt{M+1}(2N)^2(2N(M+1)))$.

For RIS deployment Problem (51), the complexity lies in solving the simplified problem (51). Assume that the interior-point method is adopted, then the complexity of the worst case is $\mathcal{O}(3+U+1)^2(2M+U+2)$. In the worst case, denote the required number of iterations for PCCA as

Algorithm 2 The BCD Algorithm to Solve Problem (35)

1: Initialize feasible $\boldsymbol{l}^0$, $\boldsymbol{\varphi}^0$, and $\boldsymbol{F}_{k,i}^0$.
2: Initialize $\boldsymbol{U}_{k,i}^{(0)}$ and $\boldsymbol{W}_{k,i}^{(0)}$ according to (33) and (36), respectively.
3: Initialize the maximum number of iterations as S_{max} and the number of iterations as $s=0$.
4: **repeat**
5: Calculate $\boldsymbol{F}_{k,i}^{(s+1)}$ by solving the convex approximations of Problem (37);
6: Calculate $\boldsymbol{\varphi}^{(s+1)}$ by solving the convex approximations of Problem (49);
7: Calculate $\{\boldsymbol{l}^{(s+1)}, \boldsymbol{U}_{k,i}^{(s+1)}, \boldsymbol{W}_{k,i}^{(s+1)}\}$ according to the PCCA Algorithm;
8: **until** $s = S_{max}$.

[2]As O^{tot} consists of two parts with different physical meanings: weighted MSE and rate, their numerical values may have more than 3 orders of magnitude difference. In this case, it is better to check these two parts separately for satisfactory performance.

This article has been accepted for publication in a future issue of this journal, but has not been fully edited. Content may change prior to final publication. Citation information: DOI10.1109/TWC.2022.3140268, IEEE Transactions on Wireless Communications

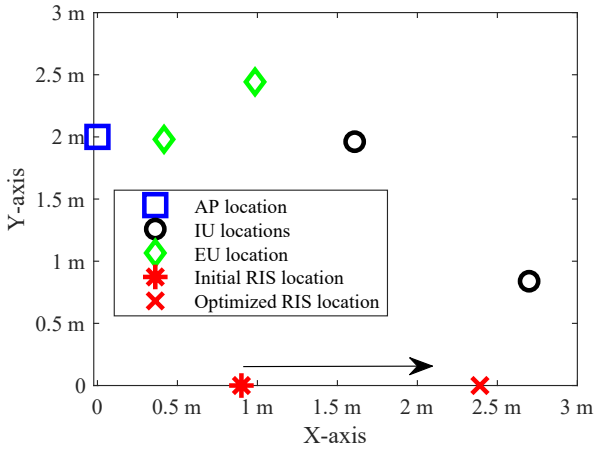

Fig. 4. The simulation scenario of the STIPT system.

N_{Max}^{PCCA}. Then, the total complexity of solving Problem (51) is $\mathcal{O}(N_{Max}^{PCCA}(3+U+1)^2 (2M+U+2))$.

Overall, the total complexity of the proposed BCD algorithm is given by $\mathcal{O}((N_F^{SCA}\sqrt{I+K}(2KIN_td)^2 2N_td(M+2) + N_{Max}^{PCCA}(3+U+1)^2(2M+U+2) + N_F^{SCA}\sqrt{I+K}(2KIN_td)^2 2N_td(M+2) + N_{Max}^{PCCA}(3+U+1)^2(2M+U+2))S_{max})$, where S_{max} denotes the maximum number of iterations.

IV. Simulation Results

Simulation results are presented in this section to evaluate the performance of the proposed algorithm. In the simulation, THz frequency range at the AP is 300-340 GHz, the bandwidth of each sub-band is 20 GHz, and the molecular absorption coefficients are generated according to [55]. The AP is located along the Y-axis with height of 2 m. The AP's transmit antenna is modelled as a uniform planar array (UPA) with size of $N_t = 5 \times 10$, and $P_t^{max} = 10$ W. The IUs and EUs are both equipped with 2 receive antennas. The antenna gain is set as $G_t = 15$ and $G_r = 6$. The separations between the transmit/receive antennas are set to be 0.1 mm. In order to verify the performance of the proposed algorithm more comprehensively, the initial locations of RIS are randomly generated in the simulations.

As shown in Fig. 4, there are 2 IUs and 2 EUs which are randomly distributed in a square area with width of 3 m. The RIS is installed on the X-axis, and the separations between the RIS reflecting elements are 0.1 mm. In Fig. 4, the number of reflecting elements is set to 100. The initial coordinate of the RIS in X-axis is marked as "$*$" and the optimized coordinate in X-axis is marked as "$\times$". It is observed that in the layout shown in Fig. 4, the optimized coordinate of the RIS is updated by the proposed BCD algorithm.

The proposed BCD algorithm given in Algorithm 2 is labelled as "PropBCD". For performance comparison, we consider two benchmark schemes:

- The first scheme which is labelled as "BeamOpt" only optimizes the transmit precoding matrices with the fixed RIS's phase shift and coordinate; This scheme can be obtained by removing step 6 and step 7 of Algorithm 2.

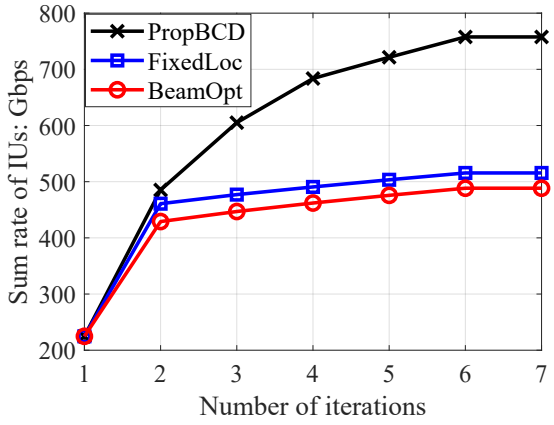

Fig. 5. The convergence performance of different algorithms.

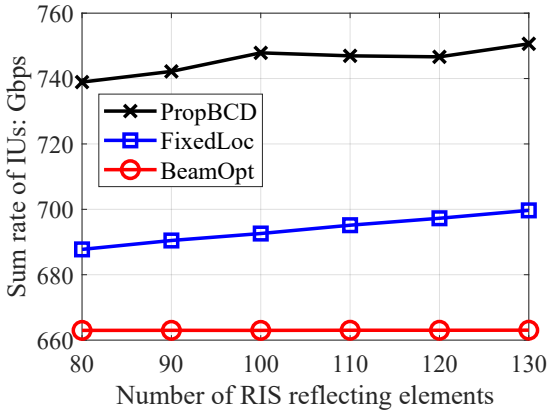

Fig. 6. The sum rate versus the number of reflecting elements.

- The scheme labelled as "FixedLoc" optimizes both the transmit precoding matrices and the RIS's phase shift, where the RIS's coordinate is kept fixed. This scheme is obtained by removing step 7 of Algorithm 2.

Fig. 5 shows the convergence performance of the proposed algorithm and the benchmarks, where its simulation scenario is shown in Fig. 4. In Fig. 5, the required harvest power by the RIS and EU are set as 0.1 mW. It is observed that the achieved sum rate of IUs increases with the number of iterations for all considered cases, and all the considered schemes converge within 7 iterations. As expected, the proposed BCD algorithm achieves the best performance. Significant rate improvement can be obtained by optimizing the RIS's coordinate.

Fig. 6 shows the achieved sum rates of IUs by different schemes versus the number of RIS reflecting elements. The simulation results are averaged over 100 random realizations, where the initial coordinate of the RIS, the IUs, and the EUs are randomly generated. As shown in Fig. 6, the sum rates of IUs achieved by the proposed BCD algorithm and the "FixedLoc" algorithm increase with the number of reflecting elements. However, the proposed BCD algorithm can achieve a higher sum rate, and the performance gap increases with the number of reflecting elements. This implies that the proposed BCD algorithm can fully exploit the potential benefits provided by the RIS, especially in this STIPT system. In addition, it

This article has been accepted for publication in a future issue of this journal, but has not been fully edited. Content may change prior to final publication. Citation information: DOI10.1109/TWC.2022.3140268, IEEE Transactions on Wireless Communications

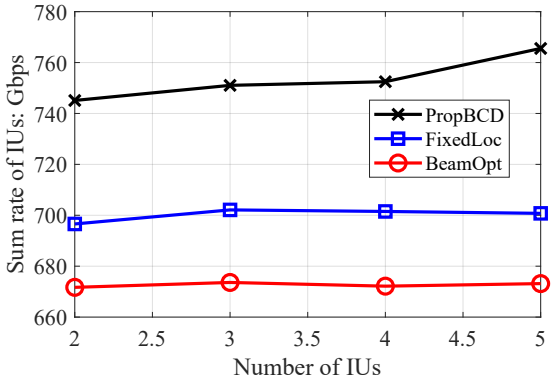

Fig. 7. The sum rate versus the number of IUs.

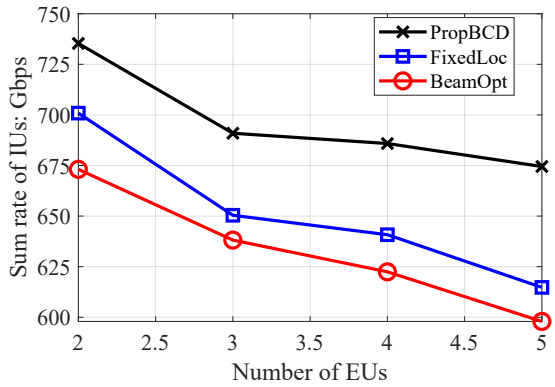

Fig. 8. The sum rate versus the number of EUs.

is observed that the sum rate of the "BeamOpt" algorithm remains the same as the number of reflecting elements increases since the RIS related parameters are not optimized in this scheme.

Fig. 7 shows the achieved sum rates of the IUs by different schemas versus the number of IUs in the system. It is interesting to see that the achieved sum rates by the "PropBCD" algorithm increases with the number of IUs. Meanwhile the sum rate obtained by the "BeamOpt" algorithm slightly increases, and that of the "FixedLoc" algorithm keeps fixed. This result clearly validates the benefits provided by the RIS in the STIPT system. By utilizing the RIS, the transmission channel can also be optimized to fully exploit the spatial diversity so that the sum rate performance can be enhanced. In particular, in the THz system, where the channel gain is very sensitive to the transmit distance, optimizing the RIS's coordinate can help provide considerable performance gain.

Fig. 8 shows the achieved sum rates of the IUs versus the number of EUs in the system, and the number of IUs is fixed to be 2. Then, it is observed that the sum rate of the IUs decreases with the number of EUs for all cases, as more power needs to be harvested for the EUs. In addition, the performance gap between the "PropBCD" algorithm and the other benchmarks increases with the number of EUs, which also shows the superiority of the proposed algorithm.

Fig. 9 shows the sum-rate performance obtained by the proposed algorithms with the imperfect user position information. In the simulations, users are located in the XOY plane. As the

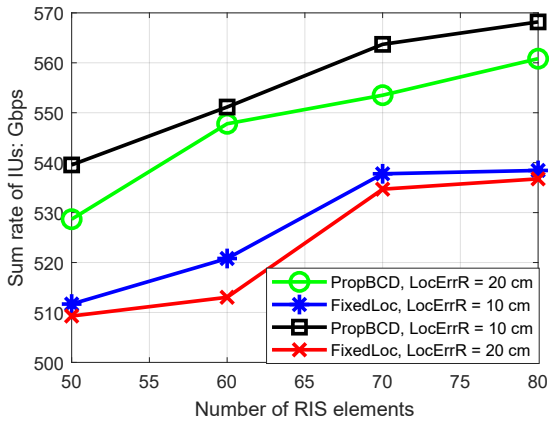

Fig. 9. The impacts of imperfect user position information.

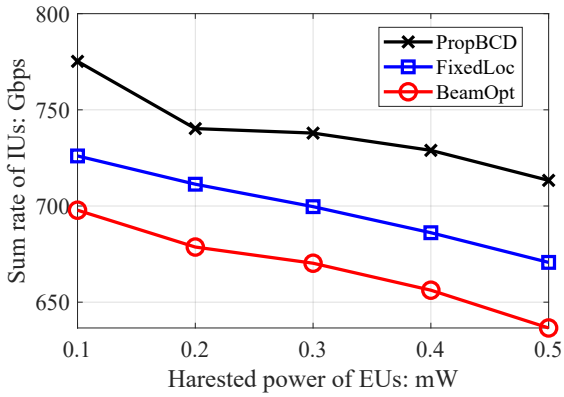

Fig. 10. The sum rate versus the harvested power of EUs.

user location information is imperfect, the position of the IU's location is uniformly distributed in a circular area. The radius of the circle for position shift is denoted as "LocErrR". As shown in Fig. 9, it is observed that the "PropBCD" algorithm still outperforms the "FixedLoc" algorithm with the imperfect user position information. In addition, the degradation of sum-rate performance increases with the error of user location information, but the performance gaps keep stable between the proposed algorithm and the compared "FixedLoc" case.

Fig. 10 shows the impact of the harvest power required by the EUs on the sum rate performance. In Fig. 10, the required

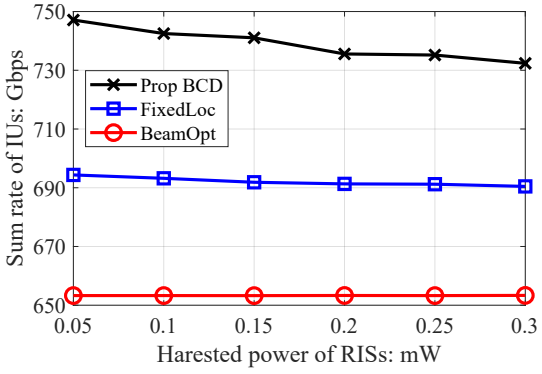

Fig. 11. The sum rate versus the harvested power of RISs

This article has been accepted for publication in a future issue of this journal, but has not been fully edited. Content may change prior to final publication. Citation information: DOI10.1109/TWC.2022.3140268, IEEE Transactions on Wireless Communications

power of the RIS is fixed to 0.1 mW, and the number of EUs is 2. It is observed that the proposed BCD algorithm outperforms the other two algorithms. As shown in Fig. 10, the achieved sum rate of IUs by the BCD algorithm decreases with the required harvested power of EUs for all considered cases. In addition, the performance gap between the "PropBCD" algorithm and the other schemes keeps stable with the required power. This implies that the proposed algorithm still has stable performance advantages when the power harvesting demand from EUs increases.

Finally, Fig. 11 shows the impact of the harvest power required by the RIS on the sum rate performance. In Fig. 11, the required power of the EU is 0.1 mW, and the other simulation parameters are the same as those of Fig. 10. As expected, the proposed BCD algorithm outperforms the other two algorithms, but the performance gap slightly decreases with the required power to harvest. It becomes more difficult to find the new coordinate of RIS to improved IU's rate while guaranteeing the more stringent harvested power constraints of RIS. Also, compared with the impact of the EU's harvested power shown in Fig. 10, RIS's required harvest power has a slighter impact on the rate performance.

V. Conclusions

This paper investigated a new simultaneous THz information and power transfer system, named STIPT, where the RIS is utilized to support the THz transmission. In this system, the RIS can utilize the power harvesting technology to self-sustain its power consumption. The optimization problem has been formulated to maximize the IUs' sum rate while guaranteeing the EU's and RIS's power harvesting requirements. A BCD-based alternating optimization algorithm has been proposed to optimize the transmit precoding for IUs, RIS's reflecting coefficients and the RIS's coordinate. Simulation results have shown that the proposed algorithm can achieve considerable performance gain in terms of the sum rate. With the assistance of RIS, the transmission channel can be optimized to fully exploit the spatial diversity so that the sum-rate performance can be enhanced. As the channel gain of the THz transmission is very sensitive to the transmission distance, optimizing the RIS's coordinate in the STIPT system can help provide considerable performance gain. For future work, the deployment of RIS will be investigated from an analytical view. Given the distribution of receivers, the presence of blocking objects will also be considered.

Acknowledgments

This work was supported in part by the National Natural Science Foundation of China under Grants 62001107, No. 61971129, No. 61960206005, No. 61871128, Basic Research Project of Jiangsu Provincial Department of Science and Technology under Grant No. BK20190339, No. Bk20192002.

Appendix A
Proof of Convexity

The Hessian matrix of $f_{k,i}(r_i, d_0)$ with respect to (r_i, d_0) is given by

$$\bigtriangledown^2 f_{k,i} = \frac{\mu_k}{r_i d_0} \exp\left(-K_k(r_u + d_0)\right) \begin{bmatrix} \frac{(K_k r_u+1)^2+1}{r_i^2} & \frac{(K_k r_u+1)(K_k d_0+1)}{r_i d_0} \\ \frac{(K_k r_u+1)(K_k d_0+1)}{r_i d_0} & \frac{(K_k d_0+1)^2+1}{d_0^2} \end{bmatrix}. \quad \text{(A.1)}$$

Then, it is observed that $\bigtriangledown^2 f_{k,i}$ is positive-definite so that $f_{k,i}^2(r_i, d_0)$ is convex with respect to (r_i, d_0). In addition, the Hessian matrix of $f_{k,i}^2(r_i, d_0)$ with respect to (r_i, d_0) is

$$\bigtriangledown^2 f_{k,i}^2 = \frac{\mu_k^2}{r_i^2 d_0^2} \exp\left(-2K_k(r_u + d_0)\right) \begin{bmatrix} \frac{(2K_k r_u+2)^2+2}{r_i^2} & \frac{(2K_k r_u+2)(2K_k d_0+2)}{r_i d_0} \\ \frac{(2K_k r_u+2)(2K_k d_0+2)}{r_i d_0} & \frac{(2K_k d_0+2)^2+2}{d_0^2} \end{bmatrix}. \quad \text{(A.2)}$$

As $\bigtriangledown^2 f_{k,i}^2$ is positive definite, $f_{k,i}^2(r_i, d_0)$ is convex with respect to (r_i, d_0).

References

[1] Z. Zhang, H. Pang, A. Georgiadis, and C. Cecati, "Wireless power transfer—an overview," *IEEE Transactions on Industrial Electronics*, vol. 66, no. 2, pp. 1044–1058, 2019.

[2] R. Zhang and C. K. Ho, "MIMO broadcasting for simultaneous wireless information and power transfer," *IEEE Transactions on Wireless Communications*, vol. 12, no. 5, pp. 1989–2001, 2013.

[3] N. Akhtar and Y. Perwej, "The internet of nano things (IoNT) existing state and future prospects," *GSC Advanced Research and Reviews*, vol. 5, no. 2, pp. 131–150, 2020. [Online]. Available: https://gsconlinepress.com/journals/gscarr/content/internet-nano-things-iont-existing-state-and-future-prospects

[4] S. Mizojiri and K. Shimamura, "Wireless power transfer via subterahertz-wave," *Applied Sciences*, vol. 8, no. 12, p. 2653, 2018. [Online]. Available: https://www.mdpi.com/2076-3417/8/12/2653

[5] L.-G. Tran, H.-K. Cha, and W.-T. Park, "RF power harvesting: a review on designing methodologies and applications," *Micro and Nano Systems Letters*, vol. 5, no. 1, pp. 1–16, 2017.

[6] Z. Rong, M. S. Leeson, M. D. Higgins, and Y. Lu, "Simultaneous wireless information and power transfer for AF relaying nanonetworks in the terahertz band," *Nano Communication Networks*, vol. 14, pp. 1–8, 2017.

[7] X. You and et al., "Towards 6G wireless communication networks: vision, enabling technologies, and new paradigm shifts," *Science China Information Sciences*, vol. 64, no. 1, pp. 1–74, 2021.

[8] M. T. Barros, R. Mullins, and S. Balasubramaniam, "Integrated terahertz communication with reflectors for 5G small-cell networks," *IEEE Transactions on Vehicular Technology*, vol. 66, no. 7, pp. 5647–5657, 2017.

[9] J. Tan and L. Dai, "THz precoding for 6G: Applications, challenges, solutions, and opportunities." [Online]. Available: https://arxiv.org/pdf/2005.10752

[10] S. Mizojiri, K. Shimamura, M. Fukunari, S. Minakawa, S. Yokota, Y. Yamaguchi, Y. Tatematsu, and T. Saito, "Subterahertz wireless power transmission using 303-GHz rectenna and 300-kW-class gyrotron," *IEEE Microwave and Wireless Components Letters*, vol. 28, no. 9, pp. 834–836, 2018.

[11] S. Mizojiri, K. Takagi, K. Shimamura, S. Yokota, M. Fukunari, Y. Tatematsu, and T. Saito, "Demonstration of sub-terahertz coplanar rectenna using 265 GHz gyrotron," in *2019 IEEE Wireless Power Transfer Conference (WPTC)*. Piscataway, NJ: IEEE, 2019.

[12] Q. Wu, S. Zhang, B. Zheng, C. You, and R. Zhang, "Intelligent reflecting surface aided wireless communications: A tutorial." [Online]. Available: http://arxiv.org/pdf/2007.02759v2

[13] M. Di Renzo, A. Zappone, M. Debbah, M.-S. Alouini, C. Yuen, J. de Rosny, and S. Tretyakov, "Smart radio environments empowered by reconfigurable intelligent surfaces: How it works, state of research, and the road ahead," *IEEE Journal on Selected Areas in Communications*, vol. 38, no. 11, pp. 2450–2525, 2020.

[14] E. Basar, M. Di Renzo, J. de Rosny, M. Debbah, M.-S. Alouini, and R. Zhang, "Wireless communications through reconfigurable intelligent surfaces," *IEEE Access*, vol. 7, pp. 116 753–116 773, 2019.

[15] S. Gong, X. Lu, D. T. Hoang, D. Niyato, L. Shu, D. in Kim, and Y.-C. Liang, "Toward smart wireless communications via intelligent reflecting surfaces: A contemporary survey," *IEEE Communications Surveys & Tutorials*, vol. 22, no. 4, pp. 2283–2314, 2020.

[16] C. Pan, H. Ren, K. Wang, J. F. Kolb, M. Elkashlan, M. Chen, M. Di Renzo, Y. Hao, J. Wang, A. L. Swindlehurst *et al.*, "Reconfigurable intelligent surfaces for 6g systems: Principles, applications, and research directions," *IEEE Communications Magazine*, vol. 59, no. 6, pp. 14–20, 2021.

[17] C. Pan, H. Ren, K. Wang, W. Xu, M. Elkashlan, A. Nallanathan, and L. Hanzo, "Multicell MIMO communications relying on intelligent reflecting surfaces," *IEEE Transactions on Wireless Communications*, vol. 19, no. 8, pp. 5218–5233, 2020.

[18] T. Bai, C. Pan, Y. Deng, M. Elkashlan, A. Nallanathan, and L. Hanzo, "Latency minimization for intelligent reflecting surface aided mobile edge computing," *IEEE Journal on Selected Areas in Communications*, vol. 38, no. 11, pp. 2666–2682, 2020.

[19] M. Cui, G. Zhang, and R. Zhang, "Secure wireless communication via intelligent reflecting surface," *IEEE Wireless Communications Letters*, vol. 8, no. 5, pp. 1410–1414, 2019.

[20] L. Dong and H.-M. Wang, "Secure MIMO transmission via intelligent reflecting surface," *IEEE Wireless Communications Letters*, vol. 9, no. 6, pp. 787–790, 2020.

[21] K. Feng, X. Li, Y. Han, S. Jin, and Y. Chen, "Physical layer security enhancement exploiting intelligent reflecting surface," *IEEE Communications Letters*, p. 1, 2020.

[22] S. Hong, C. Pan, H. Ren, K. Wang, and A. Nallanathan, "Artificial-noise-aided secure MIMO wireless communications via intelligent reflecting surface," *IEEE Transactions on Communications*, vol. 68, no. 12, pp. 7851–7866, 2020.

[23] X. Yu, D. Xu, and R. Schober, "Enabling secure wireless communications via intelligent reflecting surfaces," in *2019 IEEE Global Communications Conference (GLOBECOM)*. IEEE, 122019, pp. 1–6.

[24] Z. Chu, W. Hao, P. Xiao, and J. Shi, "Intelligent reflecting surface aided multi-antenna secure transmission," *IEEE Wireless Communications Letters*, vol. 9, no. 1, pp. 108–112, 2020.

[25] Y. Yang, B. Zheng, S. Zhang, and R. Zhang, "Intelligent reflecting surface meets OFDM: Protocol design and rate maximization," *IEEE Transactions on Communications*, vol. 68, no. 7, pp. 4522–4535, 2020.

[26] X. Ma, Z. Chen, W. Chen, Y. Chi, L. Yan, C. Han, and S. Li, "Joint hardware design and capacity analysis for intelligent reflecting surface enabled terahertz MIMO communications." [Online]. Available: https://arxiv.org/pdf/2012.06993

[27] B. Ning, Z. Chen, W. Chen, and Y. Du, "Channel estimation and transmission for intelligent reflecting surface assisted THz communications." [Online]. Available: https://arxiv.org/pdf/1911.04719

[28] X. Ma, Z. Chen, Y. Chi, W. Chen, L. Du, and Z. Li, "Channel estimation for intelligent reflecting surface enabled terahertz MIMO systems," in *2020 IEEE International Conference on Communications Workshops (ICC Workshops)*. IEEE, 2020/6/7 - 2020/6/11, pp. 1–6.

[29] A.-A. A. Boulogeorgos and A. Alexiou, "Coverage analysis of reconfigurable intelligent surface assisted THz wireless systems," *IEEE Open Journal of Vehicular Technology*, p. 1, 2021.

[30] B. Ning, Z. Chen, W. Chen, Y. Du, and J. Fang, "Terahertz multi-user massive mimo with intelligent reflecting surface: Beam training and hybrid beamforming," *IEEE Transactions on Vehicular Technology*, vol. 70, no. 2, pp. 1376–1393, 2021.

[31] W. Hao, G. Sun, M. Zeng, Z. Zhu, Z. Chu, O. A. Dobre, and P. Xiao, "Robust design for intelligent reflecting surface assisted MIMO-OFDMA terahertz communications." [Online]. Available: https://arxiv.org/pdf/2009.05893

[32] Y. Pan, K. Wang, C. Pan, H. Zhu, and J. Wang, "UAV-assisted and intelligent reflecting surfaces-supported terahertz communications." [Online]. Available: http://arxiv.org/pdf/2010.14223v1

[33] ——, "Sum rate maximization for intelligent reflecting surface assisted terahertz communications." [Online]. Available: https://arxiv.org/pdf/2008.12246

[34] Z. Feng, B. Clerckx, and Y. Zhao, "Waveform and beamforming design for intelligent reflecting surface aided wireless power transfer: Single-user and multi-user solutions." [Online]. Available: https://arxiv.org/pdf/2101.02674

[35] C. Pan, H. Ren, K. Wang, M. Elkashlan, A. Nallanathan, J. Wang, and L. Hanzo, "Intelligent reflecting surface aided MIMO broadcasting for simultaneous wireless information and power transfer," *IEEE Journal on Selected Areas in Communications*, vol. 38, no. 8, pp. 1719–1734, 2020.

[36] H. Yang, X. Yuan, J. Fang, and Y.-C. Liang, "Reconfigurable intelligent surface aided constant-envelope wireless power transfer," *IEEE Transactions on Signal Processing*, vol. 69, pp. 1347–1361, 2021.

[37] J. Liu, K. Xiong, Y. Lu, D. W. K. Ng, Z. Zhong, and Z. Han, "Energy efficiency in secure IRS-aided SWIPT," *IEEE Wireless Communications Letters*, vol. 9, no. 11, pp. 1884–1888, 2020.

[38] Z. Li, W. Chen, and Q. Wu, "Joint beamforming design and power splitting optimization in IRS-assisted SWIPT NOMA networks." [Online]. Available: https://arxiv.org/pdf/2011.14778

[39] Q. Wu and R. Zhang, "Joint active and passive beamforming optimization for intelligent reflecting surface assisted SWIPT under qos constraints," *IEEE Journal on Selected Areas in Communications*, vol. 38, no. 8, pp. 1735–1748, 2020.

[40] T. Bai, C. Pan, H. Ren, Y. Deng, M. Elkashlan, and A. Nallanathan, "Resource allocation for intelligent reflecting surface aided wireless powered mobile edge computing in OFDM systems," 2020. [Online]. Available: https://arxiv.org/pdf/2003.05511

[41] C. Han and I. F. Akyildiz, "Distance-aware bandwidth-adaptive resource allocation for wireless systems in the terahertz band," *IEEE Transactions on Terahertz Science and Technology*, vol. 6, no. 4, pp. 541–553, 2016.

[42] J. M. Jornet and I. F. Akyildiz, "Channel modeling and capacity analysis for electromagnetic wireless nanonetworks in the terahertz band," *IEEE Transactions on Wireless Communications*, vol. 10, no. 10, pp. 3211–3221, 2011.

[43] T. J. McQueen, C. Della Silva, S. G. Johnston, W. R. Barnett, C. Merrill, and J. C. Couch, "Object tracking and authentication using modular wall units," Feb. 13 2020, US Patent App. 16/362,432.

[44] B. Lyu, P. Ramezani, D. T. Hoang, S. Gong, Z. Yang, and A. Jamalipour, "Optimized energy and information relaying in self-sustainable IRS-empowered WPCN," *IEEE Transactions on Communications*, vol. 69, no. 1, pp. 619–633, 2021.

[45] M. Pengnoo, M. T. Barros, L. Wuttisittikulkij, B. Butler, A. Davy, and S. Balasubramaniam, "Digital twin for metasurface reflector management in 6G terahertz communications," *IEEE Access*, vol. 8, p. 1, 2020.

[46] S. Priebe, M. Kannicht, M. Jacob, and T. Kürner, "Ultra broadband indoor channel measurements and calibrated ray tracing propagation modeling at THz frequencies," *Journal of Communications and Networks*, vol. 15, no. 6, pp. 547–558, 2013.

[47] C. Chaccour, M. N. Soorki, W. Saad, M. Bennis, and P. Popovski, "Can terahertz provide high-rate reliable low latency communications for wireless VR?" [Online]. Available: https://arxiv.org/pdf/2005.00536

[48] A. Elzanaty, A. Guerra, F. Guidi, and M.-S. Alouini, "Reconfigurable intelligent surfaces for localization: Position and orientation error bounds." [Online]. Available: https://arxiv.org/pdf/2009.02818.pdf

[49] C. Han, A. O. Bicen, and I. F. Akyildiz, "Multi-ray channel modeling and wideband characterization for wireless communications in the terahertz band," *IEEE Transactions on Wireless Communications*, vol. 14, no. 5, pp. 2402–2412, 2015.

[50] W. Tang and et al., "Wireless communications with reconfigurable intelligent surface: Path loss modeling and experimental measurement." [Online]. Available: https://arxiv.org/pdf/1911.05326

[51] B. Lyu, P. Ramezani, D. T. Hoang, S. Gong, Z. Yang, and A. Jamalipour, "Optimized energy and information relaying in self-sustainable irs-empowered wpcn," *IEEE Transactions on Communications*, vol. 69, no. 1, pp. 619–633, 2021.

[52] D. P. Palomar, J. M. Cioffi, and M. A. Lagunas, "Joint tx-rx beamforming design for multicarrier MIMO channels: a unified framework for convex optimization," *IEEE Transactions on Signal Processing*, vol. 51, no. 9, pp. 2381–2401, 2003.

[53] M. Razaviyayn, "Successive convex approximation: Analysis and applications," Ph.D. dissertation, University of Minnesota, 2014.

[54] M. S. Lobo, L. Vandenberghe, S. Boyd, and H. Lebret, "Applications of second-order cone programming," *Linear algebra and its applications*, vol. 284, no. 1-3, pp. 193–228, 1998.

[55] A.-A. A. Boulogeorgos, E. N. Papasotiriou, and A. Alexiou, "A distance and bandwidth dependent adaptive modulation scheme for THz communications," in *IEEE 19th International Workshop on Signal Processing Advances in Wireless Communications*. IEEE, 2018, pp. 1–5.

This article has been accepted for publication in a future issue of this journal, but has not been fully edited. Content may change prior to final publication. Citation information: DOI10.1109/TWC.2022.3140268, IEEE Transactions on Wireless Communications

Yijin Pan received the B.S. and M.S degree in communication engineering from Chongqing University, Chongqing, China, in 2011 and 2014, respectively. She received the Ph.D. degrees from the School of Information Science and Engineering, Southeast University, Nanjing, China, in 2018. She visited the University of Kent, Kent, U.K., from November 2015 to November 2016. She held a International Newton Fellowship at the University of Kent, Kent, U.K., from 2019 and 2021. She currently holds a lecture position with National Mobile Communications Research Laboratory, Southeast University, Nanjing, China.

Her current research interests include D2D content caching, non-orthogonal multiple access, and mobile edge computing.

Kezhi Wang received his B.E. and M.E. degrees in School of Automation from Chongqing University, China, in 2008 and 2011, respectively. He received his Ph.D. degree in Engineering from the University of Warwick, U.K. in 2015. He was a Senior Research Officer in University of Essex, U.K. Currently he is a Senior Lecturer with Department of Computer and Information Sciences at Northumbria University, U.K. His research interests include wireless communications and machine learning.

Cunhua Pan received the B.S. and Ph.D. degrees from the School of Information Science and Engineering, Southeast University, Nanjing, China, in 2010 and 2015, respectively. From 2015 to 2016, he was a Research Associate at the University of Kent, U.K. He held a post-doctoral position at Queen Mary University of London, U.K., from 2016 and 2019.From 2019 to 2021, he was a Lecturer in the same university. From 2021, he is a full professor in Southeast University. His research interests mainly include reconfigurable intelligent surfaces (RIS), intelligent reflection surface (IRS), ultra-reliable low latency communication (URLLC) , machine learning, UAV, Internet of Things, and mobile edge computing. He serves as a TPC member for numerous conferences, such as ICC and GLOBECOM, and the Student Travel Grant Chair for ICC 2019. He is currently an Editor of IEEE Wireless Communication Letters, IEEE Communications Letters and IEEE ACCESS. He also serves as a leading guest editor of IEEE Journal of Selected Topics in Signal Processing (JSTSP) Special Issue on Advanced Signal Processing for Reconfigurable Intelligent Surface-aided 6G Networks, leading guest editor of IEEE Vehicular Technology Magazine on the special issue on Backscatter and Reconfigurable Intelligent Surface Empowered Wireless Communications in 6G, leading guest editor of IEEE Open Journal of Vehicular Technology on the special issue of Reconfigurable Intelligent Surface Empowered Wireless Communications in 6G and Beyond, and leading guest editor of IEEE ACCESS Special Issue on Reconfigurable Intelligent Surface Aided Communications for 6G and Beyond. He was a Workshop organizer in IEEE ICCC 2021 on the topic of Reconfigurable Intelligent Surfaces for Next Generation Wireless Communications (RIS for 6G Networks), and workshop organizer in IEEE Globecom 2021 on the topic of Reconfigurable Intelligent Surfaces for future wireless communications. He is currently the Workshops and Symposia officer for Reconfigurable Intelligent Surfaces Emerging Technology Initiative. He is a workshop chair for IEEE WCNC 2024.

Huiling Zhu received the B.S degree from Xidian Univeristy, Xi'an, China, and the Ph.D. degree from Tsinghua University, Beijing, China. She is currently a Reader (Associate Professor) in the School of Engineering and Digital Arts, University of Kent, Canterbury, United Kingdom. Her research interests are in the area of broadband wireless mobile communications, covering topics such as radio resource management, distributed antenna systems, MIMO, cooperative communications, device-to-device communications, and small cells and heterogeneous networks. She received the best paper award from IEEE Globecom2011, Houston. She has participated in a number of European and industrial projects in these topics and was holding European Commission Marie Curie Fellowship from 2014 to 2016. She has served as the Publication Chair for IEEE WCNC2013, Shanghai, Operation Chair for IEEE ICC2015, London, Symposium Co-Chair for IEEE Globecom2015, San Diego, and Track Co-Chair of IEEE VTC2016-Spring, Nanjing. Currently, she serves as an Editor for IEEE Transactions on Vehicular Technology.

Jiangzhou Wang (Fellow, IEEE) has been a Professor since 2005 at the University of Kent, U.K. His research interest is in the area of mobile communications. Professor Wang is a Fellow of the Royal Academy of Engineering, U.K., Fellow of the IEEE, and Fellow of the IET. He was the Technical Program Chair of the 2019 IEEE International Conference on Communications (ICC2019), Shanghai, the Executive Chair of the IEEE ICC2015, London, and the Technical Program Chair of the IEEE WCNC2013.